Neurobiology of Disease

TOM1 Regulates Neuronal Accumulation of Amyloid-β Oligomers by FcγRIIb2 Variant in Alzheimer's Disease

Youngdae Gwon,[1]* Tae-In Kam,[1,2]* Seo-Hyun Kim,[1] Sungmin Song,[1] Hyejin Park,[1,2] Bitna Lim,[1] Haneul Lee,[1] Weontae Lee,[3] Dong-Gyu Jo,[4] and Yong-Keun Jung[1]

[1]School of Biological Sciences, Seoul National University, Seoul 08826, Korea, [2]Department of Neurology, Johns Hopkins University School of Medicine, Baltimore, Maryland 21205, [3]Department of Biochemistry, College of Life Sciences and Biotechnology, Yonsei University, Seoul 03722, Korea, and [4]School of Pharmacy, Sungkyunkwan University, Suwon 16419, Korea

Emerging evidences suggest that intraneuronal Aβ correlates with the onset of Alzheimer's disease (AD) and highly contributes to neurodegeneration. However, critical mediator responsible for Aβ uptake in AD pathology needs to be clarified. Here, we report that FcγRIIb2, a variant of Fcγ-receptor IIb (FcγRIIb), functions in neuronal uptake of pathogenic Aβ. Cellular accumulation of oligomeric $A\beta_{1-42}$, not monomeric $A\beta_{1-42}$ or oligomeric $A\beta_{1-40}$, was blocked by *Fcgr2b* knock-out in neurons and partially in astrocytes. $A\beta_{1-42}$ internalization was FcγRIIb2 di-leucine motif-dependent and attenuated by TOM1, a FcγRIIb2-binding protein that repressed the receptor recycling. TOM1 expression was downregulated in the hippocampus of male 3xTg-AD mice and AD patients, and regulated by miR-126-3p in neuronal cells after exposure to $A\beta_{1-42}$. In addition, memory impairments in male 3xTg-AD mice were rescued by the lentiviral administration of TOM1 gene. Augmented Aβ uptake into lysosome caused its accumulation in cytoplasm and mitochondria. Moreover, neuronal accumulation of Aβ in both sexes of 3xTg-AD mice and memory deficits in male 3xTg-AD mice were ameliorated by forebrain-specific expression of Aβ-uptake-defective *Fcgr2b* mutant. Our findings suggest that FcγRIIb2 is essential for neuropathic uptake of Aβ in AD.

Key words: **Alzheimer's disease; Amyloid beta (Aβ); Intraneuronal Aβ; Fcγ-receptor IIb; TOM1; miR-126**

Significance Statement

Accumulating evidences suggest that intraneuronal Aβ is found in the early step of AD brain and is implicated in the pathogenesis of AD. However, the critical mediator involved in these processes is uncertain. Here, we describe that the FcγRIIb2 variant is responsible for both neuronal uptake and intraneuronal distribution of pathogenic Aβ linked to memory deficits in AD mice, showing a pathologic significance of the internalized Aβ. Further, Aβ internalization is attenuated by TOM1, a novel FcγRIIb2-binding protein. Together, we provide a molecular mechanism responsible for neuronal uptake of pathogenic Aβ found in AD.

Introduction

Alzheimer's disease (AD) is the most frequent type of senile dementia with symptoms of cognitive decline and memory loss. Accumulation of amyloid-β (Aβ) in the forebrain is the most prominent feature of AD, and Aβ production is accelerated by familial AD mutations in amyloid-β precursor protein (APP) and presenilin *1* and *2* genes (Querfurth and LaFerla, 2010). Although the extracellular amyloid deposition mainly composed of Aβ was regarded as the key feature of AD in the past, mounting evidences have shown that intraneuronal Aβ plays a key role in neurotoxicity. The presence of intraneuronal Aβ precedes the buildup of extracellular amyloid plaques in individuals with mild cognitive impairment and AD (LaFerla et al., 2007). In many AD mouse models, intraneuronal Aβ strongly correlates with the onset of memory impairment, sometimes even without extracellular Aβ load (Billings et al., 2005; Tomiyama et al., 2010; Eimer and Vassar, 2013). Moreover, AD-like neuronal defects are ame-

Received July 13, 2017; revised Aug. 16, 2018; accepted Aug. 24, 2018.

Author contributions: Y.G., T.-I.K., S.S., H.P., and Y.-K.J. designed research; Y.G., T.-I.K., S.-H.K., S.S., H.P., B.L., and H.L. performed research; Y.G., T.-I.K., S.-H.K., S.S., H.P., B.L., W.L., and D.-G.J. contributed unpublished reagents/analytic tools; Y.G., T.-I.K., S.S., B.L., and Y.-K.J. analyzed data; Y.G. and Y.-K.J. wrote the paper.

This work was supported by the BK21 program and Global PhD program to Y.G. and S.-H.K., the CRI Grant (NRF-2016R1A2A1A005005304) funded by the Ministry of Education, Science and Technology, and the Samsung Science and Technology Foundation under Project Number SSTFBA1401-16. We thank Dr. F. M. LaFerla (University of California, Irvine, CA) for providing 3xTg-AD mice, Dr. P. Davies (Albert Einstein College of Medicine, NY) for PHF1 antibody, Dr. D.J. Selkoe (Harvard Medical School, MA) for CHO and 7PA2 cells, Dr. E.H. Joe (Ajou University, Korea) for the technical assistance of primary astrocyte culture.

The authors declare no competing financial interests.

*Y.G. and T.-I.K. contributed equally to this work.

Correspondence should be addressed to Yong-Keun Jung, School of Biological Sciences, Seoul National University, 1 Gwanak-ro, Gwanak-gu, Seoul 08826, Korea. E-mail: ykjung@snu.ac.kr.

DOI:10.1523/JNEUROSCI.1996-17.2018

 0270-6474/18/389001-18$15.00/0

liorated by the modulation of intraneuronal Aβ-degrading enzymes, such as neprilysin, endothelin-converting enzymes, and nuclear inclusion a (NIa) (Marr et al., 2003; Pacheco-Quinto and Eckman, 2013; Shin et al., 2014).

Aβ is generated by a sequential cleavage of APP by β-secretase 1 and γ-secretase complex along the endocytic pathway (Haass et al., 2012). Most cleaved Aβ in the lumen of endocytic compartments is secreted extracellularly and this event is regulated by neuronal activity (Cirrito et al., 2008; Tampellini et al., 2009; Moghekar et al., 2011). Thus, a substantial portion of intraneuronal Aβ is from the re-uptake of secreted Aβ. Though a group of membrane proteins in neurons have been suggested to be a receptor of Aβ so far, receptor for advanced glycation end product (RAGE), low-density lipoprotein receptor-related protein 1 (LRP1), p75 neurotrophin receptor ($p75^{NTR}$), and α7 nicotinic acetylcholine receptor (α7nAChR) were investigated to mediate neuronal uptake of Aβ (Takuma et al., 2009; Ovsepian and Herms, 2013; Kanekiyo and Bu, 2014; Yang et al., 2014). However, the pathologic impact of RAGE is not only attributed to its neuronal expression since microglial and vascular RAGE also function during disease progression (Cai et al., 2016). In addition, AD-related phenotypes of APP transgenic mice with the Arctic and Swedish mutations, which show obvious intraneuronal Aβ, were not improved by the genetic absence of RAGE (Vodopivec et al., 2009). In addition, internalized Aβ through LRP1 and $p75^{NTR}$ is linked to the clearance pathway rather than the formation of intraneuronal Aβ pool (Kanekiyo et al., 2013; Ovsepian and Herms, 2013). In case of α7nAChR, its impact through the promotion of neuronal Aβ uptake is not validated over the cellular level (Yang et al., 2014). Thus, there is a discrepancy in understanding the deleterious role of intraneuronal Aβ with the current view on Aβ receptors.

Fcγ-receptor IIb (FcγRIIb) was originally reported to mediate negative regulation of immune reactions, including cytokine release and humoral response through engagement with activating FcγRs (Espéli et al., 2016). FcγRIIb is differentially expressed as two transcriptional variants, FcγRIIb1 and FcγRIIb2, by alternative splicing of the sixth exon of intact mRNA. Because FcγRIIb1 is excluded from the clathrin-coated pits by the insertion of amino acids encoded in the sixth exon, FcγRIIb2 solely mediates the endocytosis of ligand (Zhang and Booth, 2011). Though divergent effects between FcγRIIb1 and FcγRIIb2 on the immune complexes were well studied in immune cells, the functional difference of FcγRIIb variants in other tissues, such as brain, were poorly understood (Hunter et al., 1998; Joshi et al., 2006).

We previously discovered that FcγRIIb binds to Aβ and results in tau hyperphosphorylation through the deregulation of phosphoinositide signaling (Kam et al., 2013, 2016). This line of investigation has been extended by this study demonstrating that the neuronal FcγRIIb2 variant is critical in the neuronal uptake of pathogenic Aβ for neurotoxicity *in vitro* and in AD model mice.

Materials and Methods

Study design

Aβ internalization with regard to its peptide length and assembly status was analyzed in primary culture of neurons and astrocytes prepared from WT and *Fcgr2b* KO mice using Western blotting, immunocytochemistry, and ELISA. To find out the regulation of intraneuronal Aβ by FcγRIIb *in vivo*, we crossed 3xTg-AD mice with *Fcgr2b* KO mice or *Fcgr2b*-CytΔ Tg mice and analyzed them through Aβ ELISA and immunohistochemical detection of intraneuronal Aβ. Amelioration of impaired memory in 3× Tg-AD by forebrain neuronal expression of *Fcgr2b*-CytΔ was assessed under behavior tests including Y maze, novel object recognition, and passive avoidance. Promotion of Aβ internalization was demonstrated in SH-SY5Y cells stably expressing FcγRIIb2. Suitable numbers of samples were adapted from the previous reports using 3xTg-AD mice (Castello et al., 2012; Sykora et al., 2015). Because female mice were regarded to be responsive to behaviors dealing with novelty and anxiety due to higher corticosterone levels (Aoki et al., 2010), only male mice were used in memory tests. Data were collected and quantified by investigators with blindness.

Mice

Calcium/calmodulin-dependent protein kinase II α subunit (CaMKIIα)-driven transgene of *Fcgr2b*-CytΔ was produced as previously described (Kasahara et al., 2006). *Fcgr2b*-CytΔ that lacks cytoplasmic region of intact *Fcgr2b* was amplified by PCR and ligated into EcoRV site of pNN265. The following nucleotide sequences were used as primers for PCR: *Fcgr2b*-CytΔ-EcoRV-sense (5′-CGG ATA TCA TGG AGA GCA ACT GGA CTG TCC-3′), *Fcgr2b*-CytΔ-EcoRV-antisense (5′-CGG ATA TCC TAG GGA GAG GCA TAA TCT G-3′). The NotI cleavage product (2.2 kb) of the resulting construct contains *Fcgr2b*-CytΔ flanked by 5′-UTR with SV40 small T-antigen intron and 3′-UTR with early polyadenylation sequence, and was ligated into pMM403, which harbors CaMKIIα promoter. Injection of the SfiI-linearized construct into fertilized eggs of C57BL/6 was performed by Macrogen. The number of *Fcgr2b*-CytΔ founder mice was originally four and continuously mated >4 times with wild-type C57BL/6 to generate pure individual transgenic lines. Genomic DNAs from the tail of the offspring were subjected to PCR analysis using the primers corresponding to the CaMKIIα promoter and *Fcgr2b*-CytΔ mutant. Compared with WT mice, there were no visible differences in the phenotypes, such as body size, movement, and coordination in all transgenic mouse lines. The expressions of *Fcgr2b*-CytΔ transgene in four mouse lines at the fourth generation were examined by Western blotting. Among them, the F0#59 mouse line showed the highest expression of *Fcgr2b*-CytΔ and was selected for further maintenance and characterization. *Fcgr2b* KO and 3xTg-AD mice were previously described (Takai et al., 1996; Oddo et al., 2003). All animal experiments were performed under the guidelines of Seoul National University Institutional Animal Care and Use Committee.

Human brain samples and ethical statement

Hippocampal tissues from non-AD and AD (BraakV-VI) patients were obtained from the Harvard Brain Tissue Resource Center of McLean Hospital. This study was approved by the Institutional Review Board of Seoul National University (SNUIRB No. E1212/001-006).

ELISA

Mouse hippocampus was homogenized in Tris buffer saline (TBS; 50 mM Tris, pH 7.5, 150 mM NaCl). The insoluble pellet was reconstituted in GDN buffer (50 mM Tris, pH 8.0, 5 M guanidine hydrochloride). Hippocampal levels of $Aβ_{1-40}$ and $Aβ_{1-42}$ were measured by ELISA kit (IBL) according to the manufacturer's instructions.

Behavior tests

Y maze. Y maze contains three equal arms (32.5 cm long × 15 cm high) made of black plastic with 120° intervals. Mice were laid to the end of one arm and subjected to roam freely in the apparatus for 7 min. The arm entry was regarded as valid when the whole body including tail is completely entered into each arm. An effective alteration was counted when mouse entered three different arms consecutively. The spontaneous alteration was assessed as the ratio of the number of effective alteration to the number of total arm entry.

Novel object recognition. Novel object recognition was composed of 2 d habituation, 1 d training, and 2 d test session. All sessions were performed at the identical time in each day. To become familiar with the chamber (22 cm wide × 27 cm long × 30 cm high), mice were allowed to roam freely in there for 10 min. At training phase, two objects were placed to the upper right and lower left sides of the chamber and mice were subjected to recognize them for 7 min. During test phases, the object located in the upper right side was replaced with the novel object once a day. During training and test phase, time spent with each object was measured. Discrimination ratio was calculated by dividing T_{UR} by sum of

T_{UR} and T_{LL}, where T_{UR} and T_{LL} indicate the time spent with the object located in the upper right and lower left side of chamber, respectively.

Passive avoidance. Passive avoidance was composed of 1 d habituation, 1 d training, and 1 d test session. All sessions were performed at the identical time in each day. The apparatus (40 cm wide × 20 cm long × 20 cm high) consists of the bright compartment, which is lightened by overhead 8 W lamp and dark compartment whose floor is made of electrical grids. Two compartments are divided by a sliding door. At habitation session, mice were subjected to freely explore both compartments for 5 min. At the training session, mice initially placed into the bright compartment was shocked by foot grid (0.25 mA, 1 s) shortly after entering the dark compartment. At test session, the latency to enter the dark compartment was recorded.

Cell culture and DNA transfection

Primary cortical and hippocampal neurons were prepared from embryonic day (E)16 of mice as described previously (Kam et al., 2013). Triturated cells were grown in neurobasal medium (Invitrogen) containing 2% B27 supplement (Invitrogen), 100 U/ml penicillin (Invitrogen), 100 μg/ml streptomycin (Invitrogen), and 1% GlutaMAX-I (Invitrogen). Primary astrocytes were prepared from postnatal day 1 of mice as described previously (Kim et al., 2013). Primary astrocytes, SH-SY5Y, HT22, HEK293T and CHO cells were cultured in DMEM (HyClone) supplemented with 10% fetal bovine serum (HyClone), 100 U/ml penicillin (Invitrogen), and 100 μg/ml streptomycin (Invitrogen). Primary neurons were transfected using Lipofectamine 2000 reagent (Invitrogen), and SH-SY5Y, HT22, and HEK293T cells were transfected using Polyfect reagent (Qiagen) according to the manufacturer's instructions.

Preparation of synthetic and cell-derived oAβ

Synthetic oAβ were generated as described previously (Kam et al., 2013). Briefly, $Aβ_{1-40}$, $Aβ_{1-42}$, and FITC-$Aβ_{1-42}$ peptides lyophilized from 1,1,1,3,3,3,-hexafluoroisopropanol (rPeptide) were solubilized in DMSO at 2 mM and then diluted in PBS to final 125 μM. The Aβ freshly diluted was used as Aβ monomer. Aβ incubated at 4°C for 24 h was centrifuged at 12,000 × *g* for 10 min and the resulting supernatant was used as Aβ oligomers. Prepared synthetic oAβ was composed of low-*n* (1–4) Aβ oligomer with globular shape characterized by SDS-PAGE and atomic force microscope (Kam et al., 2013). Cell-derived Aβ was prepared from the conditioned media of CHO cells stably expressing V717F mutant APP (7PA2 cells; Courtesy of Dr. D. J. Selkoe, Harvard Medical School), as described previously (Kam et al., 2016). Cell debris was removed by the centrifugation at 230 × *g* for 10 min and subsequent supernatants were filtered using the YM-10 Centriprep centrifugal filter (Millipore), which discriminates peptides with molecular weight <10 kDa. In this preparation of cell-derived oAβ, we confirmed that low-*n* oligomers, such as trimers, were major component in 7PA2 CM. We also measured the concentration of $Aβ_{1-42}$ (51.3 ng/ml) using ELISA.

DNA construction

Mouse *Fcgr2b1* and *Fcgr2b2* cDNA were amplified by PCR and ligated into pEGFP-N1 and pDsRed-N1. Human FCGR2B2 cDNA was amplified by PCR and ligated into pCMV5c-FLAG. The following nucleotide sequences were used as the primers: *Fcgr2b*-NheI-sense (5′-CTA GCT AGC CAT GGA GAG CAA CTG GAC TGT-3′), *Fcgr2b*-KpnI-antisense (5′-GGG GTA CCC CAA TGT GGT TCT GGT AAT C-3′), FCGR2B2-BglII-sense (5′-GGA AGA TCT TCC ATG GGA ATC CTG TCA TTC TT-3′), and FCGR2B2-KpnI-antisense (5′-GGG GTA CCC AAT ACG GTT CTG GTC ATC A-3′). Mouse *Fcgr2b2* L274A/L275A mutant was generated by site-directed mutagenesis using following primers: *Fcgr2b2* L274A/L275A-sense (5′-CAC CTA CTC AGC TGC CAA GCA TCC CG-3′) and *Fcgr2b2* L274A/L275A-antisense (5′-CGG GAT GCT TGG CAG CTG AGT AGG TG-3′). Expression vectors of NIa WT and its activity dead mutant NIa D81A were provided by Dr. W. J. Park (GIST, Korea). These cDNA constructs were confirmed by DNA sequencing analysis.

RT-PCR

Total RNA was extracted from primary neurons or mouse tissues using TRI reagent (MRC) and cDNA was generated using M-MLV reverse-transcriptase (Enzynomics). To discriminate *Fcgr2b1* and *Fcgr2b2*, a pair of primers for *Fcgr2b* was designed to encompass the sixth exons. The following nucleotide sequences were used as the primers for RT-PCR: *Fcgr2b*-RT-sense (5′-CAG CGA CCT GTA GAT CTG GGA G-3′), *Fcgr2b*-RT-antisense (5′-CTT CAT CCA GGG CTT CGG GAT GC-3′), *Actb*-RT-sense (5′-GAG CTG CCT G AC GGC CAG G-3′), and *Actb*-RT-antisense (5′-CAT CTG GAA GGT GGA C-3′). We isolated the PCR products of murine *Fcgr2b1* and *Fcgr2b2* transcripts from agarose gel and confirmed them by DNA sequencing analysis.

Real-time PCR

Total RNAs were isolated using TRI reagent (Molecular Research Center) and cDNAs were generated by Moloney murine leukemia virus (M-MLV) reverse-transcriptase (Enzynomics). For PCR analysis, cDNA templates were mixed with PowerUp SYBR Green Master Mix (Applied Biosystems) and synthetic primers as followed: *TOM1* (5′-CCT CAG ATC GCC AAT GAG CA-3′, 5′-CCA GCT GGG ATG AGA GGT TG-3′). To measure mmu-miR-126-3p in the mouse hippocampus, cDNA generation and subsequent detection of endogenous miRNA were performed using HB miR Multi Assay Kit (Heim Biotek), according to the manufacturer's instruction. Real-time PCR was run on a Prism7300 (Applied Biosystems) and relative expression levels were normalized by *GAPDH* or *Rnu6b* expression under ΔΔ*Ct* method.

Subcellular fractionation

Subcellular fractionation assay was performed following the protocol described in (http://www.abcam.com/ps/pdf/protocols/subcellular_fractionation.pdf). Before subcellular fractionation, cells were briefly treated with trypsin-EDTA for 5 min to remove nonspecific Aβ from the plasma membrane. Cells were harvested by the centrifugation at 780 × *g* and then lysed in the cell fractionation buffer (in mM: 250 sucrose, 20 HEPES, pH 7.4, 10 KCl, 1.5 $MgCl_2$, 1 EDTA) by passing through 25 gauge needle. The resulting samples were placed on ice for 1 h. Nuclei and cell debris were excluded as pellets by centrifugation at 1000 × *g* for 10 min at 4°C. Mitochondria sample was isolated as a pellet by centrifugation of post-nucleus supernatants at 10,000 × *g* for 10 min at 4°C. The resulting supernatants were divided into the light membrane sample (pellet) and the cytoplasmic sample (supernatant) by centrifugation at 100,000 × *g* for 2 h at 4°C. Segregation of plasma membrane fraction was performed as described previously (Oh et al., 2012).

Western blotting and immunoprecipitation

The following antibodies were used for Western blotting and immunoprecipitation: Aβ (4G8 and 6E10, both Covance); BiP, Calnexin, CHDH, GFP, mouse FcγRIIb, TOM1, ubiquitin (Santa Cruz Biotechnology); Flotillin, GM130, TIM23, CD49b (BD Biosciences); human FcγRIIb, LC3 (Novus); α-tubulin, β-actin, APP, FLAG (Sigma-Aldrich); PHF1 (Courtesy of Dr. Peter Davies, Albert Einstein College of Medicine). Human hippocampal tissues for immunoprecipitation were solubilized in CHAPS lysis buffer (in mM: 150 NaCl, 1% CHAPS, 2 EDTA, 25 HEPES, pH 7.4). HT22 and HEK293T cell extracts for immunoprecipitation were solubilized in RIPA lysis buffer (150 mM NaCl, 0.1% SDS, 1% TX-100, 50 mM Tris, pH 7.5, 1% sodium deoxycholate).

Immunocytochemistry

Primary neurons and astrocytes were treated with 1.25 μM m$Aβ_{1-42}$ (1 μM nonlabeled m$Aβ_{1-42}$ mixed with 0.25 μM FITC-m$Aβ_{1-42}$) or o$Aβ_{1-42}$ (1 μM nonlabeled o$Aβ_{1-42}$ mixed with 0.25 μM FITC-o$Aβ_{1-42}$) for 18 h. Cells were treated with 500 μg/ml trypan blue in PBS before paraformaldehyde fixation to prevent background fluorescence outside the cells (Dementhon et al., 2012). Antibodies for MAP2b (BD Biosciences) and GFAP (Millipore) were used to stain primary neurons and astrocytes, respectively.

Immunohistochemistry

Immunohistochemical analyses of mouse brains were accomplished as described previously (Youmans et al., 2012). Brains were fixed with 4% paraformaldehyde for 48 h and dehydrated with 30% sucrose in PBS for 48 h. The 40-μm-thick floating sections were sliced on a CM1950 cryostat (Leica) and each section was allowed for antigen retrieval by incubating in 88% formic acid for 8 min. Each section was treated with 0.3% H_2O_2 for 5 min to inhibit endogenous peroxidase activity before the

3,3-diaminobenzidine (DAB) staining. The DAB staining was performed using Vector DAB Substrate Kit (Vector Laboratories) according to the manufacturer's instruction and observed under LSM700 confocal microscope (Zeiss) or IX71 inverted microscope (Olympus). Primary antibodies applied to immunohistochemistry (IHC) assays are described with catalog number and dilutions: MOAB-2 (NBP2-13075; 1:500), NSE (18-0042; 1:200), SYP (SC-9116; 1:100), and Iba1 (019-19741; 1:200). Secondary antibodies used in IHC assays are as follows: AlexaFluor 488 goat anti-rabbit IgG (H+L), AlexaFluor 594 goat anti-mouse IgG (H+L) (Invitrogen), and biotinylated anti-mouse IgG (Abcam).

Assessment of cell viability and cell death

Viable cells were stained with 0.5 μM Calcein-AM (Invitrogen), which is originally non-fluorescent but converted to fluorescent form under hydrolysis by intracellular esterases in live cells. Otherwise, cell viability was assessed using EZ-CyTox cell viability kit (Daeil Lab Service). Cell death in HT22 cells were assessed by counting GFP-positive cells showing apoptotic fractured nuclei characterized by ethidium homodimer-1 (Molecular Probe).

Cell-based functional screening

The cell-based functional screening was performed on the basis of the previous study (Lee et al., 2015). In the primary screening, HT22 cells were cotransfected with pEGFP-N1 and each of 120 cDNAs encoding endo-lysosomal proteins for 24 h and treated with 5 μM oAβ_{1-42} for 36 h. Cells with apoptotic blebbing or shrunk morphology were regarded as dead cells. Two independent experiments were performed and the mean values were calculated (see Fig. 4*A*). Furthermore, regulation of oAβ_{1-42}-triggered cell death by the cDNA clones was analyzed by Western blotting using caspase-3 antibody.

miRNA

The miRNA mimic negative control, hsa-miR-126-mimic, anti-miR-negative control, anti-hsa-miR-126-5p, and anti-hsa-miR-126-3p were purchased (Bioneer). Transfection of miRNA mimic constructs (final 25 nM) and anti-miR constructs (final 250 nM) was performed using Lipofectamine 2000 reagent (Invitrogen) according to the manufacturer's instruction.

Stereotaxic injection of lentivirus

Human *TOM1* ORF was amplified by PCR using synthetic primers: *TOM1* (5′-AAG TCC ATG CGG CCG CAT GGA CTT TCT CCT GGG GAA-3′, 5′-GAG GAT CCT CAT AAG GCA AAC AGC ATG T-3′). The PCR products were inserted into NotI/BamHI sites of CSII-EF-MCS-IRES-Venus, and nontarget lentivirus pLV[Exp]-EGFP:T2A:Puro-EF1A>mCherry and *TOM1* lentivirus (Vectorbuilder) were produced. The stereotaxic injection of lentivirus (1.79×10^9 transduction unit/ml) into the dentate gyrus (5 μl per hemisphere) was performed with the coordinates: anteroposterior (AP) = 2.1 mm, mediolateral (ML) = ±1.8 mm, and dorsoventral (DV) = 2.0 mm from bregma. Y maze, novel objective recognition, and passive avoidance tests were performed after 3 weeks of injection and the hippocampi were dissected for Western blotting.

Statistics

All statistical analyses were performed with SPSS. Comparisons between two means were performed by unpaired two-tailed *t* test. Comparisons among multiple mean values were performed by one-way ANOVA with Bonferroni, Tukey's, or least significant difference (LSD) *post hoc* test as indicated.

Results

FcγRIIb is an essential receptor for neuronal uptake of Aβ$_{1-42}$ oligomers

To quantify intracellular Aβ, we used a subcellular fractionation assay after extracellular Aβ treatment to primary neurons. Consistent with the previous studies (LaFerla et al., 2007; Takuma et al., 2009), Aβ was found largely in the membrane-enclosing organelles, including endocytic compartments, as well as in the cytoplasm and mitochondria (Fig. 1*A*). Then, monomeric Aβ$_{1-42}$ (mAβ$_{1-42}$) and oligomeric Aβ$_{1-42}$ (oAβ$_{1-42}$) were prepared and assessed for their internalization into primary cultured neurons and astrocytes (Fig. 1*B*). Interestingly, oAβ$_{1-42}$ was preferentially internalized into primary neurons, whereas mAβ$_{1-42}$ was internalized by primary astrocytes. Consistent with this observation, confocal microscopy showed that FITC-oAβ$_{1-42}$ and FITC-mAβ$_{1-42}$ were found mainly inside primary neurons and astrocytes, respectively, when cells were incubated with FITC-labeled Aβ$_{1-42}$ (Fig. 1*C–E*). These results illustrate that oAβ$_{1-42}$ is preferentially internalized into primary neurons relative to mAβ$_{1-42}$.

We then evaluated the relevance of FcγRIIb function in cellular uptake of Aβ species because we previously reported that FcγRIIb acts as a receptor for oAβ$_{1-42}$ in the AD brains (Kam et al., 2013). The results revealed that oAβ$_{1-42}$ was internalized into WT cortical neurons but not into *Fcgr2b* KO cortical neurons (Fig. 2*A*). Similar pattern and level of oAβ$_{1-42}$ uptake were also observed in WT and *Fcgr2b* KO astrocytes. Compared with oAβ$_{1-42}$, however, mAβ$_{1-42}$ uptake was predominant in primary astrocytes and was not much affected by *Fcgr2b* KO. Consistently, it was revealed that FITC-oAβ$_{1-42}$ internalization was also declined by *Fcgr2b* KO in MAP2b-positive hippocampal neurons, whereas FITC-mAβ$_{1-42}$ was not significantly internalized as assayed with immunocytochemistry of neuron-enriched cultures (Fig. 2*B*,*C*). Comparison of the kinetics revealed that oAβ$_{1-42}$ uptake over time was delayed by *Fcgr2b* KO in neurons (Fig. 2*D*,*E*); internalized Aβ was detected at 1.5 h after treatment in WT neurons and at 12 h in *Fcgr2b* KO neurons. Moreover, oligomeric forms of Aβ$_{1-40}$ (oAβ$_{1-40}$) that are qualitatively different from oAβ$_{1-42}$ were not internalized into primary neurons compared with oAβ$_{1-42}$ (Fig. 2*F*). Furthermore, by using the conditioned media of 7PA2 cells, which secrete soluble Aβ oligomers (Walsh et al., 2002), we found that FcγRIIb could internalize Aβ$_{1-42}$, but not Aβ$_{1-40}$ (Fig. 2*G*,*H*). The results suggest that FcγRIIb is crucial for neuronal uptake of oAβ$_{1-42}$ over mAβ$_{1-42}$ or oAβ$_{1-40}$.

In addition, neuronal uptake of Aβ was blocked by addition of purified FcγRIIb extracellular domain (FcγRIIb-ED) to the culture medium (Fig. 2*I*). Furthermore, Aβ internalization was enhanced by the overexpression of FcγRIIb or FcγRIIb Ig1 mutant, but not by deletion mutant of FcγRIIb Ig2 domain, which was reported to be critical for the interaction with oAβ$_{1-42}$ (Kam et al., 2013; Fig. 2*J*). Together, these results illustrate that the binding of oAβ$_{1-42}$ to FcγRIIb is required for Aβ internalization and neurotoxicity.

Alleviation of AD-related pathologies in 3Tg-AD mice by neuron-specific expression of Aβ uptake-defective *Fcgr2b* mutant

To address the role of neuronal FcγRIIb in the AD pathology, we generated transgenic mice that express *Fcgr2b*-deletion mutant (*Fcgr2b*-CytΔ Tg) only in forebrain neurons under the control of the CaMKIIα promoter. The *Fcgr2b*-CytΔ mutant consists of the extracellular domain and transmembrane region but lacks the cytoplasmic region of FcγRIIb and is predicted to be defective in Aβ uptake and compete with the endogenous FcγRIIb for binding to Aβ. We confirmed that oAβ$_{1-42}$-induced neurotoxicity was reduced by the expression of *Fcgr2b*-CytΔ in HT22 hippocampal cells (Fig. 3*A*). As expected, the expression of *Fcgr2b*-CytΔ in the Tg mice was restricted to the forebrain regions, including the cortex and hippocampus (Fig. 3*B*). Comparison of *Fcgr2b* expression levels with the immunoprecipitation assay showed that *Fcgr2b*-CytΔ protein level was quite comparable to that of FcγRIIb in the *Fcgr2b*-CytΔ Tg mice (Fig. 3*C*). In the

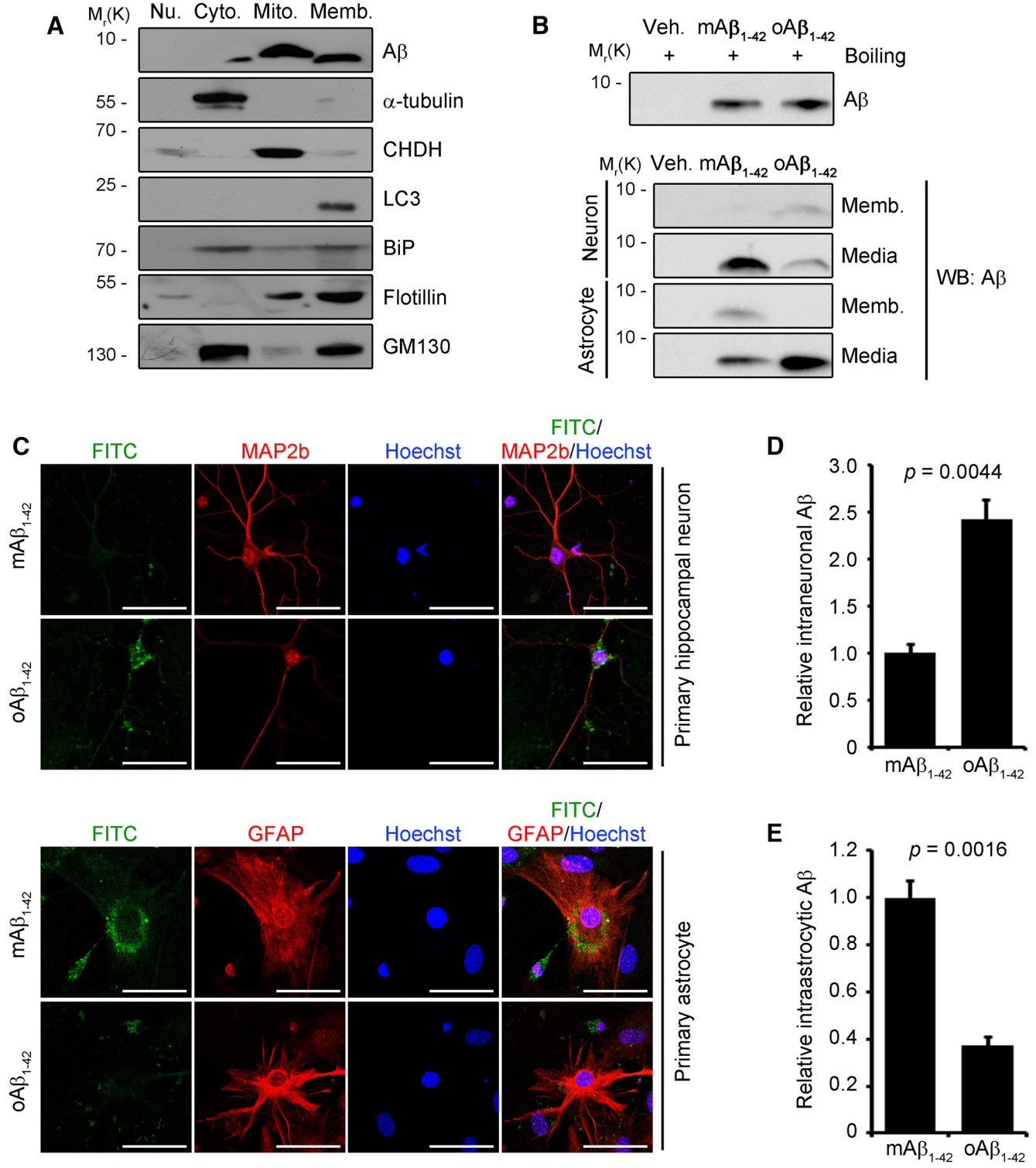

Figure 1. Preferential uptake of $A\beta_{1-42}$ oligomers over $A\beta_{1-42}$ monomer in primary neurons. ***A***, Establishment of an assay determining internalized $A\beta$ level based on subcellular fractionation. SH-SY5Y cells were treated with 2.5 μM $oA\beta_{1-42}$ for 1.5 h and then subjected to subcellular fractionation analysis. All samples (Nu, Nucleus; Cyto, cytoplasm; Mito, mitochondria; Memb, light membrane) were confirmed by Western blotting using CHDH (mitochondria), LC3 (autophagosome), BiP (ER), Flotillin (lipid raft), and GM130 (Golgi apparatus) antibodies. ***B***, Preferential uptake of $oA\beta_{1-42}$ in primary neurons. Primary mouse hippocampal neurons and astrocytes were treated with vehicle (Veh), 1 μM $mA\beta_{1-42}$, or 1 μM $oA\beta_{1-42}$ for 12 h. The light membrane samples (Memb) and conditioned media (Media) were investigated by Western blotting using $A\beta$ antibody. ***C***, Representative confocal images of internalized $mA\beta_{1-42}$ and $oA\beta_{1-42}$ in primary neurons and astrocytes. Primary murine hippocampal neurons at 10 d *in vitro* (DIV) and astrocytes were incubated with 1.25 μM $mA\beta_{1-42}$ (1 μM nonlabeled $mA\beta_{1-42}$ mixed with 0.25 μM FITC-$mA\beta_{1-42}$) or 1.25 μM $oA\beta_{1-42}$ (1 μM nonlabeled $oA\beta_{1-42}$ mixed with 0.25 μM FITC-$oA\beta_{1-42}$) for 18 h. Neurons and astrocytes were then analyzed by immunocytochemistry using MAP2b and GFAP antibodies, respectively. Scale bar, 50 μm. ***D***, ***E***, Quantification of FITC-$A\beta_{1-42}$ signal intensity in primary neurons (***D***) and astrocytes (***E***). Error bars depict mean ± SEM. $t_{(5)} = -5.45$ ($n = 3$ for monomer-treated WT neurons and $n = 4$ for oligomer-treated WT neurons, two-tailed t test) in ***D***. $t_{(6)} = 7.08$ ($n = 4$, two-tailed t test) in ***E***.

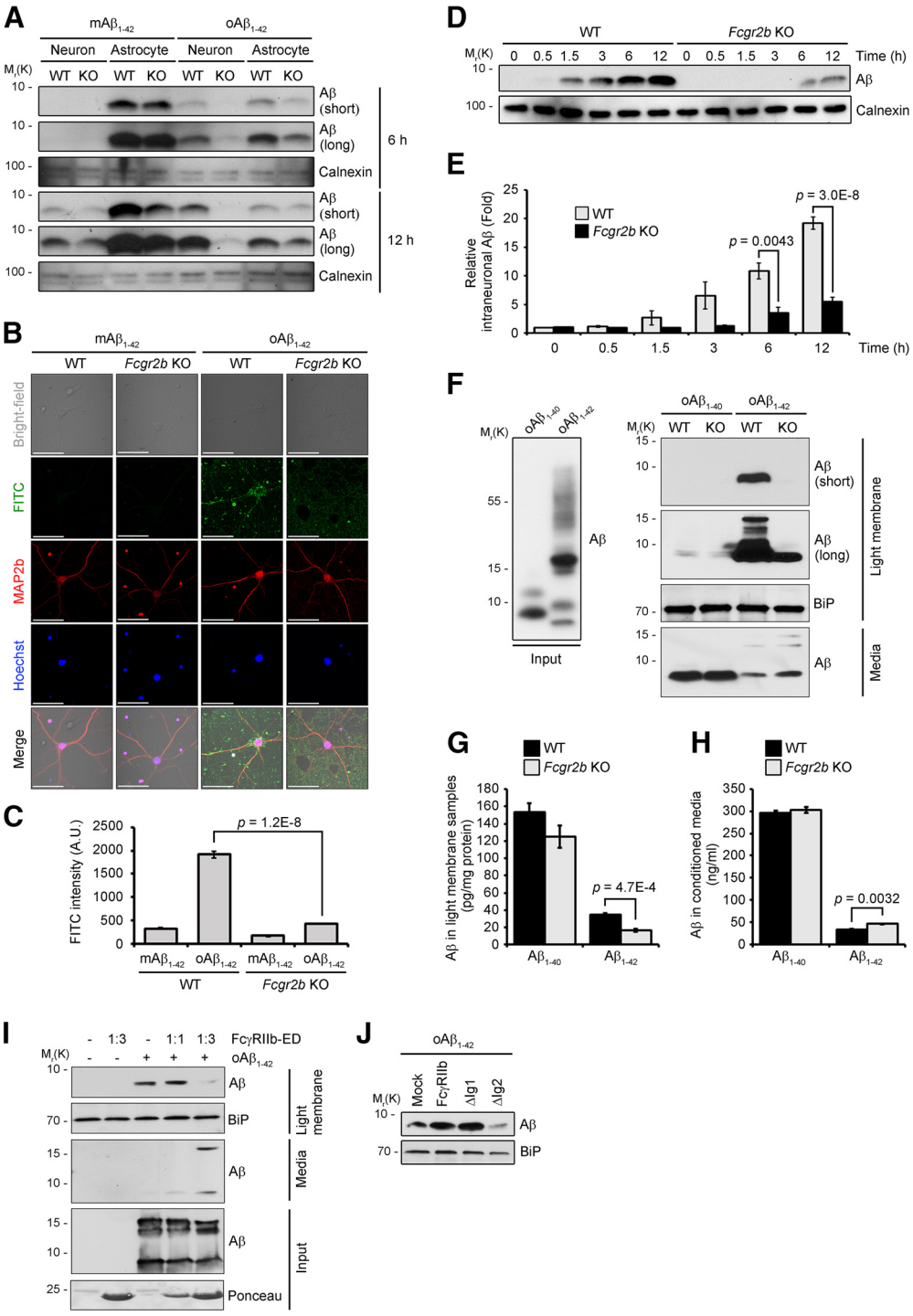

Figure 2. FcγRIIb is required for neuronal uptake of Aβ_{1-42} oligomers. ***A***, Involvement of FcγRIIb in the neuronal uptake of Aβ_{1-42} oligomers. Primary cortical neurons and primary astrocytes at 10 DIV from WT and *Fcgr2b* KO mice were treated with 1 μM mAβ_{1-42} or oAβ_{1-42} for 6 and 12 h. Intracellular Aβ level in the light membrane sample was determined. Images were taken by 10 s (short) and 60 s (long) exposure time. ***B***, ***C***, Intracellular accumulation of oAβ_{1-42} in WT MAP2b-positive hippocampal neurons but not in *Fcgr2b* KO neurons. Primary neurons were incubated with 1.25 μM mAβ_{1-42} (1 μM nonlabeled mAβ_{1-42} mixed with 0.25 μM FITC-mAβ_{1-42}) or 1.25 μM oAβ_{1-42} (1 μM nonlabeled oAβ_{1-42} mixed with 0.25 μM FITC-oAβ_{1-42}) for 18 h. Scale bar, 50 μm. Comparison of intraneuronal FITC-Aβ_{1-42} signals of WT and *Fcgr2b* KO neurons (***C***). Error bars depict mean ± SEM. $F_{(3,9)} = 357.32$ ($n = 3$ for monomer-treated WT and KO neurons and oligomer-treated KO neurons, $n = 4$ for oligomer-treated WT neurons, one-way ANOVA with Bonferroni *post hoc* test). ***D***, ***E***, Time-dependent internalization of oAβ_{1-42} by FcγRIIb. Primary neurons were incubated with 1 μM oAβ_{1-42} for the indicated times. Error bars depict mean ± SEM. $F_{(11,36)} = 23.11$ ($n = 4$, one-way ANOVA with Bonferroni *post hoc* test). ***F***, Preferential uptake of oAβ_{1-42} over oAβ_{1-40} by FcγRIIb. One microgram of Aβ_{1-40} and Aβ_{1-42} peptides was allowed to form oligomers at 4°C and analyzed by SDS-PAGE followed by Western blotting using 6E10 antibody (left). WT and *Fcgr2b* KO primary cortical neurons at 10 DIV were treated with 1 μM oAβ_{1-40} or oAβ_{1-42} for 1.5 h (right). ***G***, ***H***, Cortical neurons were incubated for 24 h with conditioned media prepared from 7PA2 cells. Aβ_{1-40} and Aβ_{1-42} in the light membrane samples (***G***) and conditioned media (***H***) were measured by ELISA. Error bars depict mean ± SEM. $F_{(3,8)} = 59.06$ (***G***) and $F_{(3,8)} = 53.09$ (***H***; $n = 4$, one-way ANOVA with Bonferroni *post hoc* test). ***I***, Binding of oAβ_{1-42} to FcγRIIb is indispensable for its uptake. SH-SY5Y cells were incubated with 1 μM oAβ_{1-42} alone or together with 3 mg (1:1) or 9 mg (1:3) purified FcγRIIb–ED protein for 1.5 h. ***J***, Requirement of FcγRIIb Ig2 domain in oAβ_{1-42} internalization. SH-SY5Y cells were transfected with pEGFP-N1 (Mock), pFcγRIIb2-GFP, pFcγRIIb2 Ig1 deletion mutant-GFP (ΔIg1), or pFcγRIIb2 Ig2 deletion mutant-GFP (ΔIg2) for 24 h and treated with 1 μM oAβ_{1-42} for 1.5 h. The light membrane samples were examined by Western blotting. For ***A***, ***D***, ***E***, ***F***, ***I***, and ***J***, the amounts of calnexin and BiP were measured as the loading control.

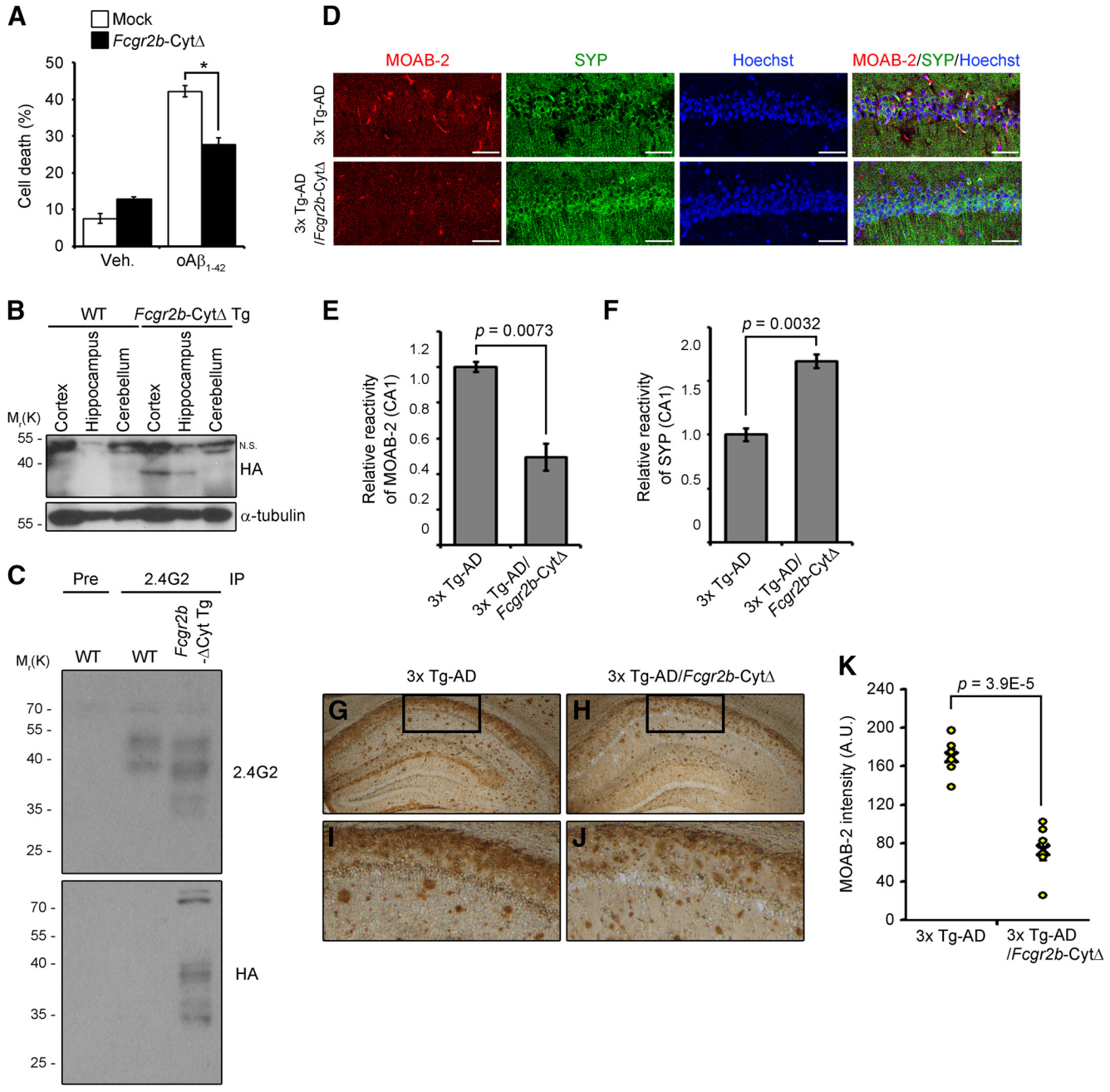

Figure 3. Decrease of intraneuronal MOAB-2 signals by neuron-specific *Fcgr2b*-CytΔ transgene in 3xTg-AD mice. ***A***, Inhibition of oAβ_{1-42}-elicited cell death by the expression of *Fcgr2b*-CytΔ. HT22 cells were transfected with pEGFP-N1 (GFP) or pFcγRIIb-CytΔ-GFP (*Fcgr2b*-CytΔ) for 12 h and then treated with 5 μM oAβ_{1-42}. *$p < 0.05$ ($n = 3$, two-tailed t test). ***B***, Forebrain neuron-specific expression of *Fcgr2b*-CytΔ transgene by CaMKIIα promoter. Cortex, hippocampus, and cerebellum of WT and *Fcgr2b*-CytΔ Tg mice at the age of 3 months were analyzed by Western blotting. ***C***, Comparison of FcγRIIb2 and *Fcgr2b*-ΔCyt expression in *Fcgr2b*-ΔCyt Tg mouse neurons. Cell extracts prepared from primary cortical neurons of WT and *Fcgr2b*-ΔCyt Tg mice were immunoprecipitated (IP) with 2.4G2 antibody and subjected to Western blotting. ***D–F***, Immunodetection of neuronal Aβ with MOAB-2 antibody in the CA1 region of hippocampus of 8 month-old 3x-Tg AD and 3x-Tg AD/*Fcgr2b*-CytΔ Tg mice. Representative confocal images were displayed, magnifying power = 200×. Scale bar (in ***D***), 50 μm. MOAB-2 (***E***) and synaptophysin (SYP; ***F***) immunoreactivities in the hippocampal CA1 region were quantified. Error bars depict mean ± SEM. $t_{(4)} = 5.033$ (***E***) and $t_{(4)} = -6.347$ (***F***; $n = 3$, two-tailed t test). ***G–J***, Immunohistochemical detection of intraneuronal Aβ in the hippocampal regions of 15 month-old 3xTg-AD (***G***, ***I***) and 3xTg-AD/*Fcgr2b*-CytΔ Tg (***H***, ***J***) mice using MOAB-2 antibody. Representative images, magnifying power = 64×. ***K***, MOAB-2 immunoreactivities in the hippocampal CA1 regions were measured by densitometric analysis. Error bars depict mean ± SEM. $t_{(10)} = 6.96$ ($n = 6$, two-tailed t test).

assay, both FcγRIIb and *Fcgr2b*-CytΔ proteins were detected as multiple bands on the acrylamide gel possibly due to the glycosylation after translation.

To verify whether Aβ uptake and memory deficits were dependent on the FcγRIIb in neurons, we crossed *Fcgr2b*-CytΔ Tg mice with 3xTg-AD model mice that display the early accumulation of intraneuronal Aβ with memory decline before extracellular amyloid deposition and neurofibrillary tangle formation (Oddo et al., 2003). Then, we examined the presence of neuronal Aβ in the brains of 3xTg-AD mice and 3xTg-AD/*Fcgr2b*-CytΔ Tg mice with IHC using MOAB-2 antibody that recognizes the first 4 aa of Aβ and theoretically could bind to APP, C99, and Aβ, but hardly interacts with APP and APP-CTF in both cells and animal models (Youmans et al., 2012; Koss et al., 2016). We also tested the preferential binding of MOAB-2 to Aβ in that MOAB-2 immunoreactivity was decreased after the administration of DAPT,

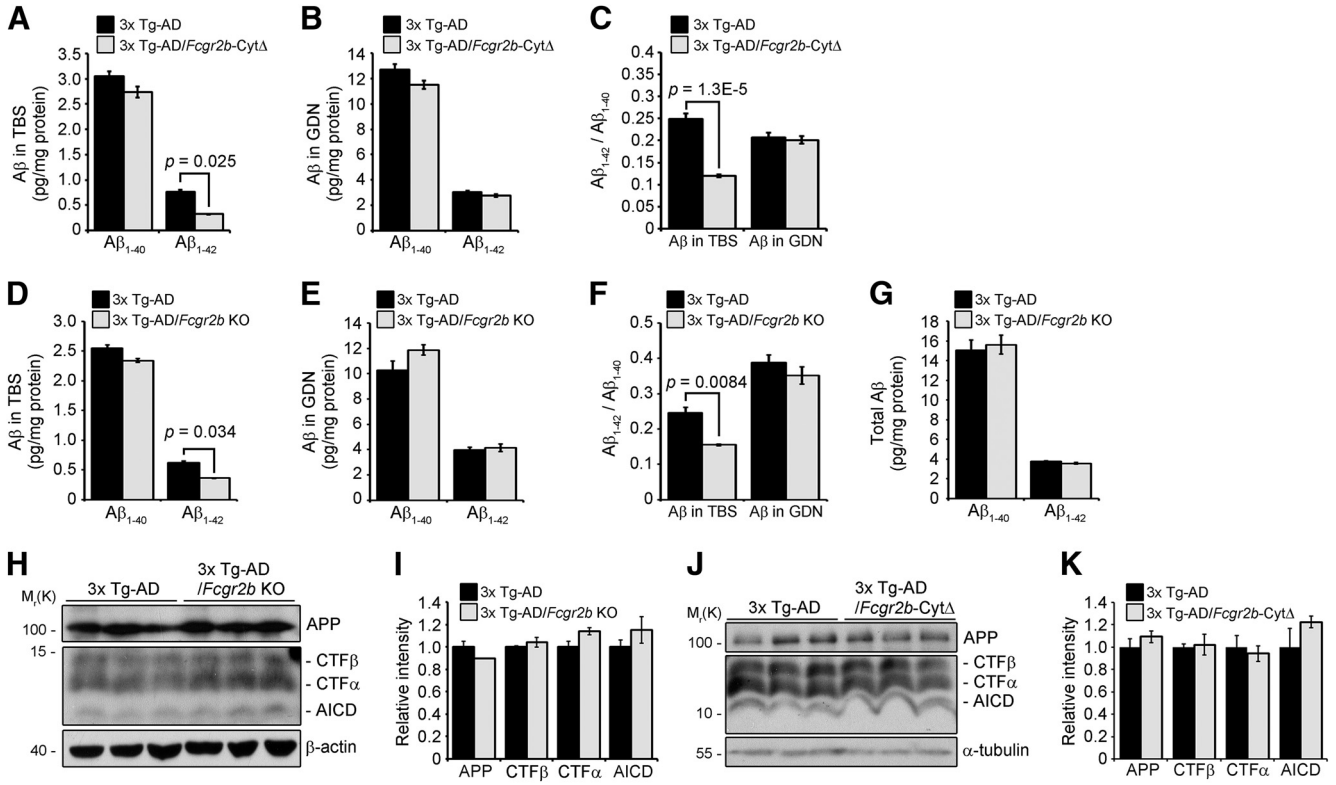

Figure 4. Reduction of soluble Aβ_{1-42} by neuronal expression of *Fcgr2b*-CytΔ or genetic deletion of *Fcgr2b* in 3xTg-AD mice. ***A–C***, The concentrations of Aβ_{1-40} and Aβ_{1-42} in the hippocampal extracts prepared in TBS (***A***) or 5 M guanidine hydrochloride (GDN; ***B***) from 3xTg-AD and 3xTg-AD/*Fcgr2b*-CytΔ mice at 8 months of age ($n = 4$) were measured. Aβ_{1-42}/Aβ_{1-40} ratios in (***A***) and (***B***) were calculated (***C***). Error bars depict mean ± SEM. $F_{(3,12)} = 251.88$ (***A***), $F_{(3,12)} = 277.97$ (***B***), and $F_{(3,12)} = 24.91$ (***C***; $n = 4$, one-way ANOVA with Bonferroni *post hoc* test). ***D–F***, Reduction of soluble Aβ_{1-42}, not insoluble Aβ_{1-42}, by *Fcgr2b* KO in 3xTg-AD mice. The hippocampal extracts of 7-month-old 3xTg-AD and 3xTg-AD/*Fcgr2b* KO mice were prepared in TBS (***D***) or 5 M GDN (***E***), and the concentrations of Aβ_{1-40} and Aβ_{1-42} were then measured. Aβ_{1-42}/Aβ_{1-40} ratios were calculated in (***F***). Error bars depict mean ± SEM. $F_{(3,12)} = 115.52$ (***D***), $F_{(3,12)} = 66.41$ (***E***), and $F_{(3,12)} = 27.37$ (***F***; $n = 4$, one-way ANOVA with LSD *post hoc* test). ***G***, No differences in total hippocampal Aβ levels between 3xTg-AD and 3xTg-AD/*Fcgr2b* KO mice. The hippocampal extracts of 7-month-old 3xTg-AD and 3xTg-AD/*Fcgr2b* KO mice were homogenized in 5 M GDN and the concentrations of Aβ_{1-40} and Aβ_{1-42} were then measured by ELISA. ***H***, ***I***, Levels of APP, APP-CTFα (CTFα), APP-CTFβ (CTFβ), and AICD in the hippocampus of both 3xTg-AD and 3xTg-AD/*Fcgr2b*-CytΔ mice at the age of 8 months ($n = 3$). ***J***, ***K***, Levels of APP, APP-CTFα (CTFα), APP-CTFβ (CTFβ), and AICD in the hippocampus of both 3xTg-AD and 3xTg-AD/*Fcgr2b* KO mice at the age of 7 months ($n = 3$).

a γ-secretase inhibitor, in 3xTg-AD mice (data not shown). Forebrain expression of *Fcgr2b*-CytΔ mutant did not alter the levels of MOAB-2-positive signals in the hippocampal CA1 region of 4-month-old 3xTg-AD mice (data not shown). On the contrary, there was a significant reduction in MOAB-2-immunoreactivity in the same region of 3xTg-AD/*Fcgr2b*-CytΔ Tg mice compared with that of 3xTg-AD mice at the age of 8 months (Fig. 3*D*,*E*) and 15 months (Fig. 3*G–K*), indicating that the accumulation of neuronal Aβ in 3xTg-AD mice requires FcγRIIb.

We further analyzed alteration of the overall Aβ levels in the AD mouse model with ELISA. As reported (Kanekiyo et al., 2013), soluble Aβ species, such as Aβ oligomers, were extracted from hippocampal tissues of the mice with TBS, and insoluble Aβ species, such as Aβ fibrils and plaques, with guanidine hydrochloride. The results of ELISA showed that the level of soluble Aβ_{1-42}, but not Aβ_{1-40}, was significantly lower in the hippocampus of 3xTg-AD/*Fcgr2b*-CytΔ Tg mice than 3xTg-AD mice at 7 months of age (Fig. 4*A*). On the contrary, there was no difference in the levels of insoluble Aβ_{1-40} and Aβ_{1-42} between 3xTg-AD and 3xTg-AD/*Fcgr2b*-CytΔ Tg mice (Fig. 4*B*). Consequently, the prominent difference in the ratio of Aβ_{1-42} to Aβ_{1-40} between 3xTg-AD and 3xTg-AD/*Fcgr2b*-CytΔ Tg mice was observed in the soluble fraction (Fig. 4*C*). The level of soluble Aβ_{1-42}, but not soluble Aβ_{1-40} and insoluble Aβ_{1-40} or Aβ_{1-42} (Fig. 4*D*,*E*), the ratio of Aβ_{1-42} to Aβ_{1-40} in the soluble fraction (Fig. 4*F*), and total Aβ level (Fig. 4*G*), were also significantly reduced in the hippocampus of 3xTg-AD mice by *Fcgr2b* gene deletion. We confirmed that the levels of full-length APP, APP C-terminal fragment α (APP-CTFα), APP C-terminal fragment β (APP-CTFβ), and APP intracellular domain (AICD) are not changed by the neuronal expression of *Fcgr2b*-CytΔ or genetic ablation of *Fcgr2b* in 3xTg-AD mice (Fig. 4*H–K*). These results indicate that FcγRIIb KO reduces soluble Aβ_{1-42} in the hippocampus of 3xTg-AD mice without altering APP processing.

Because the intraneuronal and soluble oAβ_{1-42} have long been implicated in the memory deficits of AD (Billings et al., 2005; Shankar et al., 2008), we evaluated memory function in these mice. Analysis of the memory tasks revealed that 3xTg-AD/*Fcgr2b*-CytΔ Tg mice exhibited better spatial recognition function than 3xTg-AD mice in Y-maze test (Fig. 5*A*). Memory deficit in object recognition of 3xTg-AD mice assessed by novel object recognition test was ameliorated by the neuronal expression of *Fcgr2b*-CytΔ (Fig. 5*B*). In addition, defects in learning the connection between aversive foot shock and dark chamber in 3xTg-AD mice were rescued by *Fcgr2b*-CytΔ expression (Fig. 5*C*). IHC assay revealed that the immunoreactivity against synaptophysin, a synaptic marker, was restored in 3xTg-AD mice by the expression of *Fcgr2b*-CytΔ transgene (Fig. 3*D*,*F*). We believe that intraneuronal Aβ is detected over 4 months of age and reaches to a higher level at 7 months of age accompanying memory deficits in 3xTg-AD mice. Collectively, the neuronal function of FcγRIIb contributes to AD-like pathology, including learning

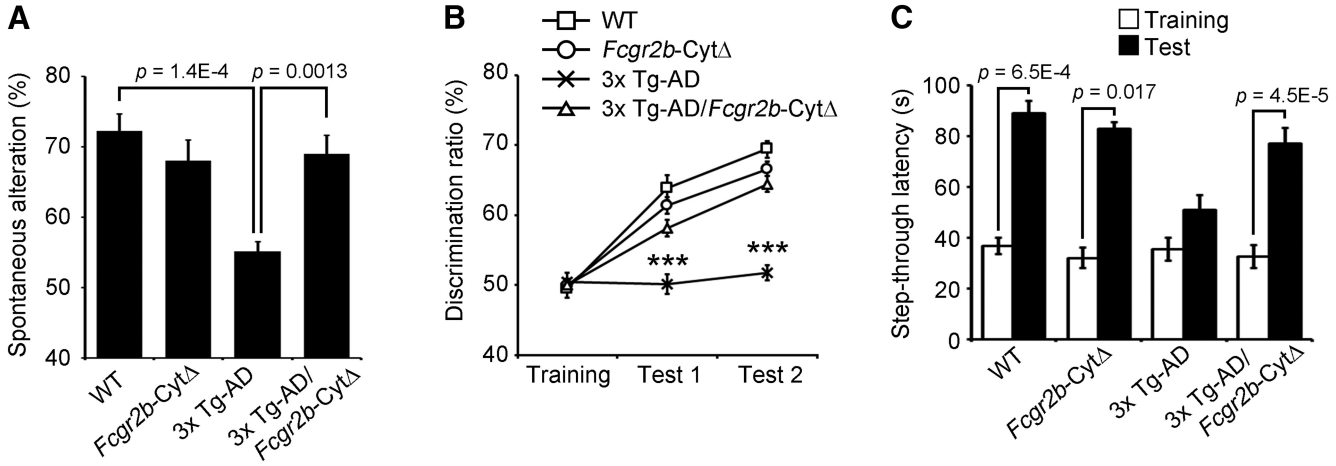

Figure 5. Alleviation of cognitive impairment by neuronal expression of *Fcgr2b*-CytΔ in 3xTg-AD mice. ***A–C***, The Y maze (***A***), novel object recognition (***B***), and passive avoidance (***C***) tests were performed in 7-month-old mice. Error bars depict mean ± SEM. $F_{(3,36)} = 9.63$ (***A***), $F_{(11,108)} = 38.93$ (***B***), and $F_{(7,72)} = 10.72$ (***C***). ***$p < 0.001$ ($n = 9$ male mice for WT and *Fcgr2b*-CytΔ Tg mice, $n = 11$ male mice for 3xTg-AD and 3xTg-AD/*Fcgr2b*-CytΔ mice, one-way ANOVA with Bonferroni *post hoc* test).

and memory impairments, in 3xTg-AD mice with the accumulation of neuronal $A\beta_{1-42}$.

Promotion of $oA\beta_{1-42}$ uptake of via a FcγRIIb2 variant is linked to neurotoxicity

Interestingly, in the mouse brain, we found an alternative splicing variant of FcγRIIb, FcγRIIb2, which has high activity in the receptor-mediated endocytosis, by sequencing cDNA generated from FcγRIIb transcript (Hunziker and Fumey, 1994). FcγRIIb2 mRNA was exclusively detected in the hippocampus and cortex, whereas FcγRIIb1 mRNA was found in the spleen and thymus (Fig. 6*A*). In particular, FcγRIIb2 mRNA was dramatically increased in the $oA\beta_{1-42}$-treated primary neurons (Fig. 6*B*). Examination of the FcγRIIb2 activity revealed that cellular uptake of $oA\beta_{1-42}$ was enhanced by the stable expression of FcγRIIb2 in SH-S Y5Y cells, while $A\beta_{1-42}$ in the culture media was concomitantly reduced (Fig. 6*C–E*). Notably, the ability of FcγRIIb2 to uptake $oA\beta_{1-42}$ was higher than FcγRIIb1 in HT22 and SH-SY5Y cells (Fig. 6*F*). In accordance with the results observed in *Fcgr2b* KO neurons, internalization of $oA\beta_{1-42}$ over $oA\beta_{1-40}$ was selectively promoted by *FcγRIIb2* expression in SH-SY5Y cells (Fig. 6*G*). Thus, FcγRIIb2 functions to efficiently internalize $oA\beta_{1-42}$ into neurons.

To address how FcγRIIb2 internalizes $oA\beta_{1-42}$, we first focused on the di-leucine motif, which is critical for the endocytosis of immune complex (Hunziker and Fumey, 1994), in the cytoplasmic domain of FcγRIIb2. We substituted the 274th and 275th leucine residues with alanine (L274A/L275A) and validated this mutant. Unlike FcγRIIb2 WT, $oA\beta_{1-42}$ uptake was not stimulated by FcγRIIb2 L274A/L275A expression (Fig. 6*H*). Because *Fcgr2b* KO neurons have been shown to be resistant to Aβ neurotoxicity (Kam et al., 2013) and lack of intraneuronal Aβ (Fig. 2*B*), we performed an inverse analysis. Although the overexpressed FcγRIIb2 WT and FcγRIIb2 L274A/L275A themselves did not affect cell viability, only FcγRIIb2 WT, but not FcγRIIb2 L274A/L275A or FcγRIIb1, decreased cell viability in the presence of $oA\beta_{1-42}$ (Fig. 6*I*). In addition, treatment with monodansylcadaverine (MDC), an inhibitor of clathrin-mediated endocytosis (Chen et al., 2009), suppressed $oA\beta_{1-42}$-induced cell death and $oA\beta_{1-42}$ internalization in HT22 cells (Fig. 6*J*). Together, these results suggest that the di-leucine motif-dependent activity of FcγRIIb2 is essential for Aβ uptake and neurotoxicity.

FcγRIIb2-mediated Aβ uptake is negatively regulated by TOM1

We further characterized the FcγRIIb2-mediated Aβ uptake by isolating regulator(s) involved in this process. We established a cell-based assay for $oA\beta_{1-42}$ neurotoxicity and screened a cDNA expression library encoding endo-lysosome-resident proteins. From the screening, Target of Myb 1 (TOM1) was the most potent in suppressing $oA\beta_{1-42}$-induced neurotoxicity in primary neurons and HT22 cells (Fig. 7*A–C*). Ectopic expression of TOM1 also suppressed cell death triggered by ER stress, which is downstream of FcγRIIb in $oA\beta_{1-42}$ neurotoxicity (Kam et al., 2013), but not by oxidative stress and tumor necrosis factor-α (TNFα)/cycloheximide (Fig. 7*D*). Interestingly, $oA\beta_{1-42}$ uptake into SH-SY5Y cells and FcγRIIb2-mediated $oA\beta_{1-42}$ uptake were all inhibited by TOM1 expression (Fig. 7*E*), whereas FcγRIIb2-mediated $oA\beta_{1-42}$ uptake was enhanced by TOM1 knockdown (Fig. 7*F*), indicating that TOM1 negatively regulates cellular uptake and neurotoxicity of $oA\beta_{1-42}$.

We next assessed how TOM1 regulated Aβ uptake. Coimmunoprecipitation assay revealed that FcγRIIb2-FLAG bound to HA-TOM1 in the transfected cells and vice versa (Fig. 7*G*,*H*). In addition, we found that endogenous FcγRIIb2 bound to TOM1 in HT22 cells and this interaction was weakened by $oA\beta_{1-42}$ treatment (Fig. 7*I*). To determine a pathophysiological relevance of this observation, we analyzed the FcγRIIb2-TOM1 interaction in AD brains. We found that FcγRIIb2 bound to TOM1 in the hippocampal lysates of non-AD controls and this interaction was significantly diminished in AD brains (Fig. 7*J*). Thus, we hypothesize that the interaction of TOM1 to FcγRIIb2 is crucial to regulate Aβ uptake during AD progression.

To address the function of TOM1 in regulating the FcγRIIb-mediated Aβ uptake, we analyzed subcellular localization of FcγRIIb dependent on the expression of TOM1 and Aβ treatment. Because endocytosed FcγRIIb2 goes through the recycling pathway to the plasma membrane (Bergtold et al., 2005), we hypothesized that TOM1 may regulate FcγRIIb2 translocation along the endocytic pathway. In SH-SY5Y cells, FcγRIIb2 was found in the Rab7-positive late endosome after $oA\beta_{1-42}$ treatment. However, this subcellular localization of FcγRIIb2 was decreased by TOM1 knockdown (Fig. 8*A*). On the contrary, FcγRIIb2 located in the recycling and Rab11a-positive endosome was increased by TOM1 knockdown (Fig. 8*B*). We also found that

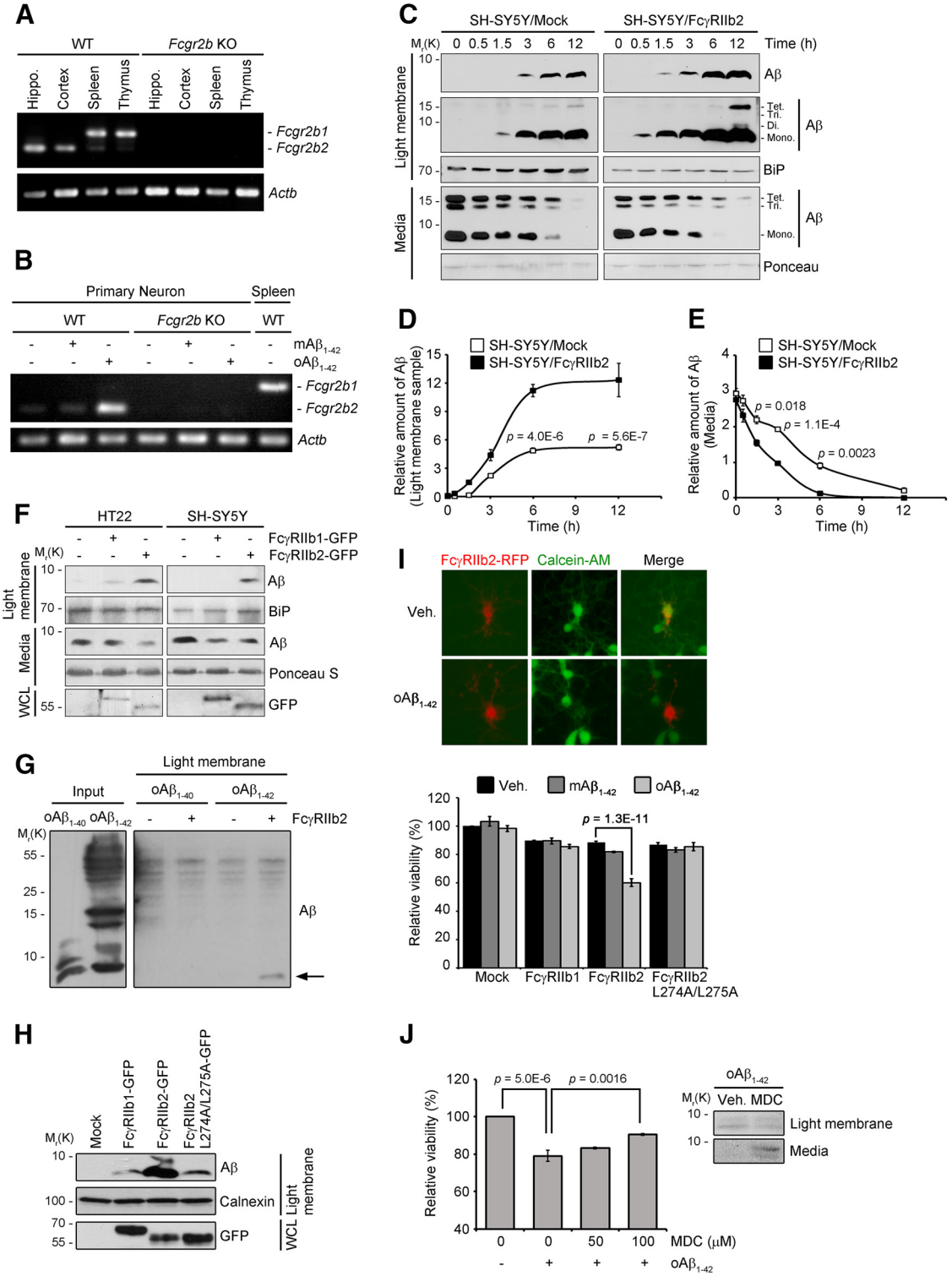

Figure 6. Endocytosis-promoting activity of FcγRIIb2 variant enhances neuronal uptake of and cell death by oAβ_{1-42}. ***A***, Expression pattern of FcγRIIb2 in the brain tissues. Total RNAs isolated from the hippocampus (Hippo), cortex, spleen, and thymus of WT and *Fcgr2b* KO mice were analyzed by RT-PCR. ***B***, Neuronal expression of the FcγRIIb2 variant revealed by RT-PCR. WT and *Fcgr2b* KO primary cortical neurons were treated with 1 μM mAβ_{1-42} or oAβ_{1-42} for 24 h. ***C–E***, Increased internalization of oAβ_{1-42} by FcγRIIb2 stable expression. The amounts of Aβ in the light membrane samples and conditioned media (Media) were examined with Western blotting (***C***). The signals of Aβ on the blots in light membrane samples (***D***) and Media (***E***) were measured and normalized by the loading control BiP and Ponceau S, respectively. Points on line plots depict mean ± SEM. $F_{(11,24)} = 54.78$ (***C***) and $F_{(11,24)}$ 101.51 (***D***; $n = 3$, one-way ANOVA with Bonferroni *post hoc* test). ***F***, FcγRIIb2-mediated cellular uptake of oAβ_{1-42}. HT22 and SH-SY5Y cells were transfected with pEGFP-N1, pFcγRIIb1-EGFP, or pFcγRIIb2-EGFP for 36 h, and treated with 1 μM oAβ_{1-42} for 1.5 h. Aβ levels in the light membrane samples and conditioned media (Media) were determined by Western blotting. Transfection efficiency was determined by Western blotting of whole-cell lysate (WCL) using GFP antibody. ***G***, Distinct uptake of oAβ_{1-42} and oAβ_{1-40} via FcγRIIb2. SH-SY5Y cells were transfected with pEGFP-N1 or pFcγRIIb2 for 36 h and treated with 1 μM oAβ_{1-42} for 1.5 h. Aβ levels in the light membrane samples were determined by Western blotting as in ***F***. ***H***, FcγRIIb2 di-leucine residues critical in Aβ uptake. SH-SY5Y cells were transfected with the indicated constructs for 24 h and treated with 1 μM oAβ_{1-42} for 6 h. Whole-cell lysates (WCL) and the light membrane samples prepared by subcellular fractionation were analyzed by Western blotting. ***I***, Enhanced uptake of Aβ by FcγRIIb2 is associated with neuronal death. Cortical neurons were transfected with the constructs for 24 h and incubated with vehicle (Veh), 1 μM mAβ_{1-42}, or 1 μM oAβ_{1-42} for 36 h. Viable cells were stained with 0.5 μM Calcein-AM (top). Error bars depict mean ± SD. $F_{(11,24)} = 65.27$ ($n = 3$, one-way ANOVA with Bonferroni (*Figure legend continues.*)

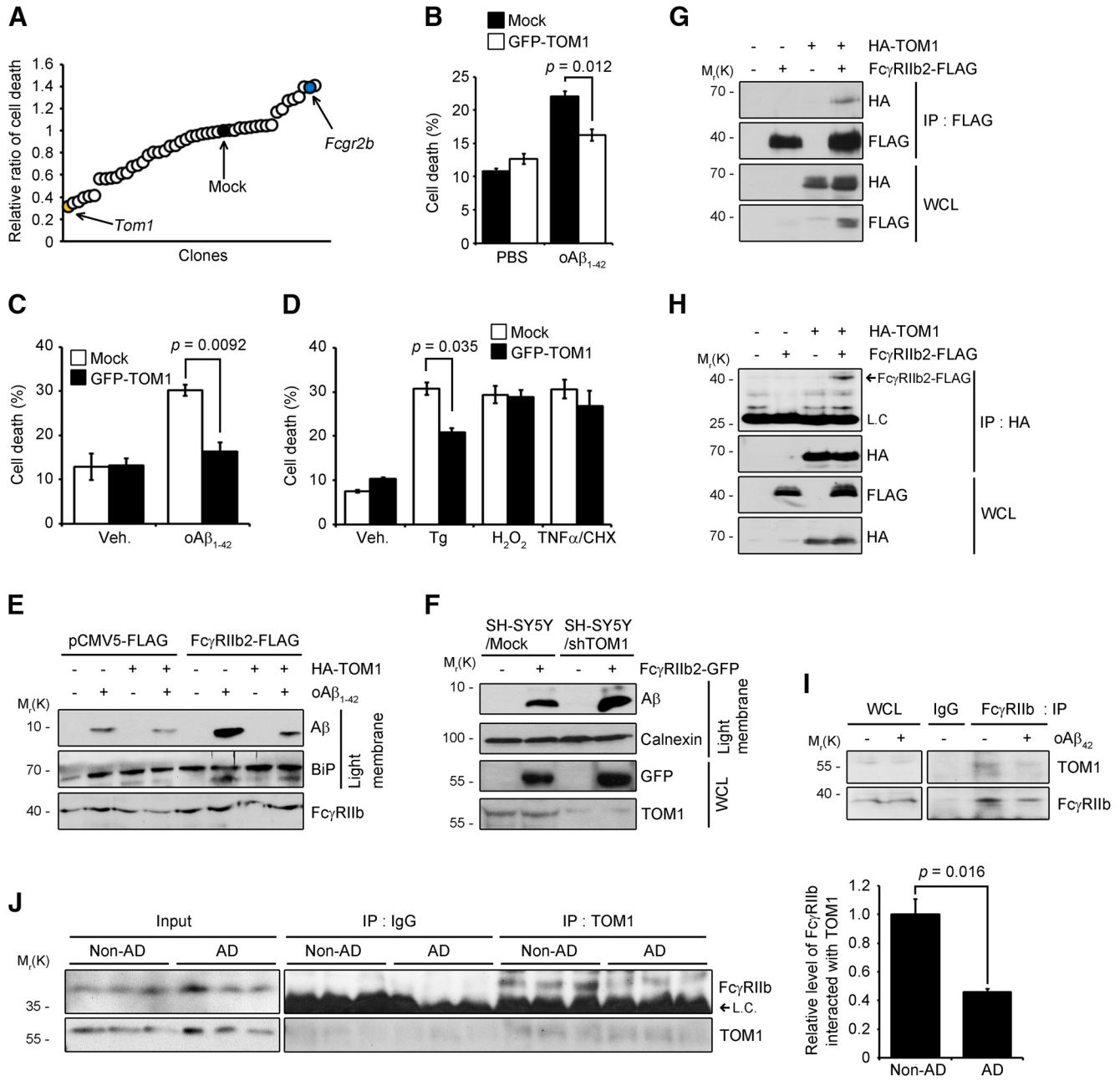

Figure 7. TOM1 binds to FcγRIIb2 and restrains Aβ internalization. ***A***, Dot plot analysis describing cell-based functional screening to isolate modulators of oAβ_{1-42}-induced neurotoxicity in HT22 cells. ***B***, Inhibition of oAβ_{1-42}-induced neuronal death by TOM1. Primary hippocampal neurons transfected with pEGFP-C1 (Mock) or pEGFP-TOM1 were incubated with 5 μM oAβ_{1-42} for 36 h. Error bars depict mean ± SD. $F_{(3,8)} = 29.59$ ($n = 3$, one-way ANOVA with Bonferroni *post hoc* test). ***C***, ***D***, Inhibition of oAβ_{1-42}- and ER stress-induced neuronal death by TOM1. HT22 cells were transfected with pEGFP-C1 (Mock) or pEGFP-TOM1 for 16 h and treated with 5 μM oAβ_{1-42} for 36 h (***C***) or thapsigargin (Tg) for 12 h, 300 μM H_2O_2 for 18 h or both 30 ng/ml TNF-α and 10 μg/ml cycloheximide (CHX) for 18 h (***D***). Error bars depict mean ± SEM. $F_{(3,8)} = 15.36$ (***C***) and $F_{(7,16)} = 27.14$ (***D***; $n = 3$, one-way ANOVA with Bonferroni *post hoc* test). ***E***, Inhibition of FcγRIIb2-mediated Aβ uptake by TOM1. SH-SY5Y cells were transfected with pFcγRIIb2-FLAG and treated with 1 μM Aβ_{1-42} for 1.5 h. ***F***, Enhancement of FcγRIIb2-mediated Aβ uptake by TOM1 knockdown. SH-SY5Y stable cells expressing pSUPER-neo (Mock) or pTOM1 shRNA (shTOM1) were transfected with pFcγRIIb2-GFP for 48 h and treated with oAβ_{1-42} for additional 3 h. Whole-cell lysates (WCLs) and the light membrane samples were analyzed by Western blotting. ***G***, H FcγRIIb2-FLAG interacts with HA-TOM1. HEK293T cells were transfected with pFcγRIIb2-FLAG and pHA-TOM1 for 24 h and subjected to immunoprecipitation (IP) assay using FLAG (***G***) or HA (***H***) antibody. ***I***, Blockade of the FcγRIIb-TOM1 interaction by oAβ_{1-42}. HT22 cells were treated with oAβ_{1-42} and then IP using IgG or FcγRIIb antibody. ***J***, Decreased interaction between FcγRIIb2 and TOM1 in the hippocampus of AD patients. Hippocampal lysates were subjected to IP assay (left). Level of TOM1-interacting FcγRIIb on the blots were quantified (right). Error bars depict mean ± SEM. $t_{(4)} = 3.99$ ($n = 3$, two-tailed *t* test). For ***E*** and ***F***, the amounts of BiP and calnexin were measured as the loading control of light membrane samples.

←

(*Figure legend continued.*) *post hoc* test; bottom). ***J***, Suppression of oAβ_{1-42}-induced neurotoxicity by the inhibition of clathrin-mediated endocytosis. SH-SY5Y cells were pre-incubated with 100 μM MDC for 1 h and then treated with 1 μM oAβ_{1-42} for 36 h (left) or 12 h (right). Cell death rates and the Aβ levels in the light membrane samples and conditioned media (Media) were determined. Error bars depict mean ± SEM. $F_{(3,12)} = 32.86$ ($n = 4$, one-way ANOVA with Bonferroni *post hoc* test). For ***F*** and ***H***, the amounts of calnexin were measured as the loading control of light membrane samples.

FcγRIIb2 located in the plasma membrane was markedly increased by TOM1 knockdown in SH-SY5Y cells, whereas FcγRIIb2 was internalized into the post-plasma membrane fraction in response to Aβ (Fig. 8*C*), arguing that the increment of FcγRIIb2 recycling to the plasma membrane in TOM1-deficient cells may facilitate oAβ_{1-42} uptake. Thus, TOM1 functions to regulate FcγRIIb2-associated endocytosis by altering the trafficking of receptor recycling.

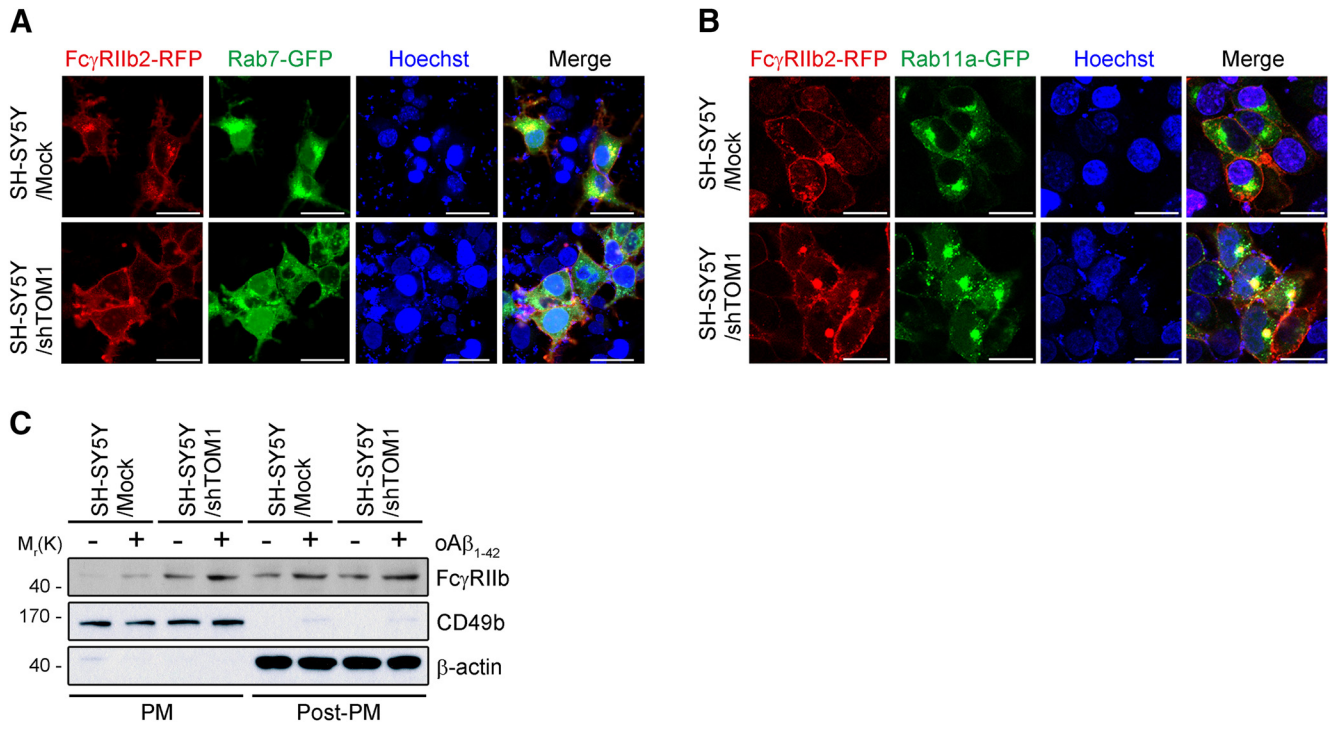

Figure 8. Membrane-retargeting of endocytosed FcγRIIb2 is regulated by TOM1. ***A***, ***B***, Targeting of endocytosed FcγRIIb2 to recycling endosome is enhanced by TOM1 knockdown. SH-SY5Y/Mock and SH-SY5Y/shTOM1 cells were transfected with pFcγRIIb2-RFP and either pRab7-GFP (***A***) or pRab11a-GFP (***B***) for 24 h and incubated with 1 μM oAβ_{1-42} for 6 h. ***C***, Localization of FcγRIIb2 to plasma membrane is elevated by TOM1 knockdown. SH-SY5Y/Mock and SH-SY5Y/shTOM1 cells were treated with PBS or 1 μM oAβ_{1-42} for 12 h. Cells were subjected to fractionation assay to prepare plasma membrane (PM) and post-plasma membrane (Post-PM). CD49b serves as plasma membrane marker in Western blotting. Scale bar, 20 μm.

TOM1 level is regulated by miR-126-3p and crucial for memory rescue in 3xTg-AD mice

Compared with non-AD controls, we found that TOM1 level was marginally reduced in the hippocampus of patients with AD (Fig. 9*A*). Moreover, compared with age-matched control mice, TOM1 protein was reduced in the hippocampus of 3xTg-AD mice at 6 months of age (Fig. 9*B*). We also found that both levels of TOM1 protein and *TOM1* transcripts were decreased in SH-SY5Y cells following exposure to oAβ_{1-42} (Fig. 9*C*,*D*). It was previously reported that miR-126 targets 3′-UTR of TOM1 mRNA to regulate its expression and may be involved in several neuropsychiatric disorders (Oglesby et al., 2010; Sonntag et al., 2012; Kim et al., 2014) and that miR-126 expression potentiates Aβ toxicity (Kim et al., 2016). Thus, we attempted to identify whether miR-126 regulated TOM1 level in AD model. As expected, TOM1 level in SH-SY5Y cells was downregulated by the transfection with the mimicry of hsa-miR-126 (Fig. 9*E*). Along with this regulation, we found that oAβ_{1-42} internalization was enhanced by the expression of hsa-miR-126 (Fig. 9*F*).

To examine the relation between miR-126 and TOM1 expression in response to oAβ_{1-42}, we inhibited the expression of endogenous miR-126 with two anti-miR oligonucleotides, which target the 5p and 3p strands of miR-126, respectively. Restoration of TOM1 expression was observed in oAβ_{1-42}-treated cells by the transfection of anti-miR-126-3p only (Fig. 9*G*), suggesting that miR-126-3p is a specific regulator of TOM1. More, we found that miR-126-3p level was significantly increased in the hippocampus of 3xTg-AD mice compared with age-matched WT controls (Fig. 9*H*). Together, the results illustrate a role of miR-126-3p engaged in TOM1 regulation, which is important in the FcγRIIb2-mediated internalization of oAβ_{1-42} in AD models.

We then addressed whether memory deficits in 3xTg-AD mice could be affected by complementing TOM1 expression. When the TOM1-expressing lentivirus was injected into the dentate gyrus of 6- to 7-month-old WT and 3xTg-AD mice, the levels of TOM1 were elevated approximately twofold in the hippocampus of the mice (Fig. 10*A*–*C*). On the other hand, there was no significant change in the level of APP. When we measured memory function, deficits in cognitive functions of 3xTg-AD mice, as examined with Y-maze, novel object recognition, and passive avoidance tests, were mitigated by the injection of the TOM1-expressing lentivirus (Fig. 10*D*–*F*). These results illustrate a pathologic significance of TOM1 expression in the AD-related memory deficits of 3xTg-AD mice.

Massive influx of Aβ into lysosome elicits Aβ overflow to other compartments

To address how the internalized Aβ exhibits neurotoxicity, we assessed degradation event of the internalized Aβ. As reported (Caglayan et al., 2014), the inhibition of lysosomal activity with bafilomycin A1 (Baf A1), a vacuolar-type H^+-ATPase inhibitor, resulted in the accumulation of FITC-oAβ_{1-42} in the DND-99-positive lysosomes of SH-SY5Y cells (Fig. 11*A*). As a comparable control, prevention of receptor-mediated endocytosis with MβCD showed accumulation of FITC-oAβ_{1-42} on the plasma membrane. Again, fractionation assay following brief exposure to oAβ_{1-42} revealed that degradation of the internalized Aβ was blocked by the treatment with Baf A1 or 3-MA, an autophagy inhibitor, but not by MG132, a proteasome inhibitor (Fig. 11*B*). Hence, most of the internalized Aβ is degraded in the lysosome. Actually, a low dose of intraneuronal oAβ_{1-42} was rapidly degraded at an early time without affecting cell viability. In contrast, treatment of high and neurotoxic dose of oAβ_{1-42} resulted in a drastic accumulation of oAβ_{1-42} in the lysosome (Fig. 11*C*). Sim-

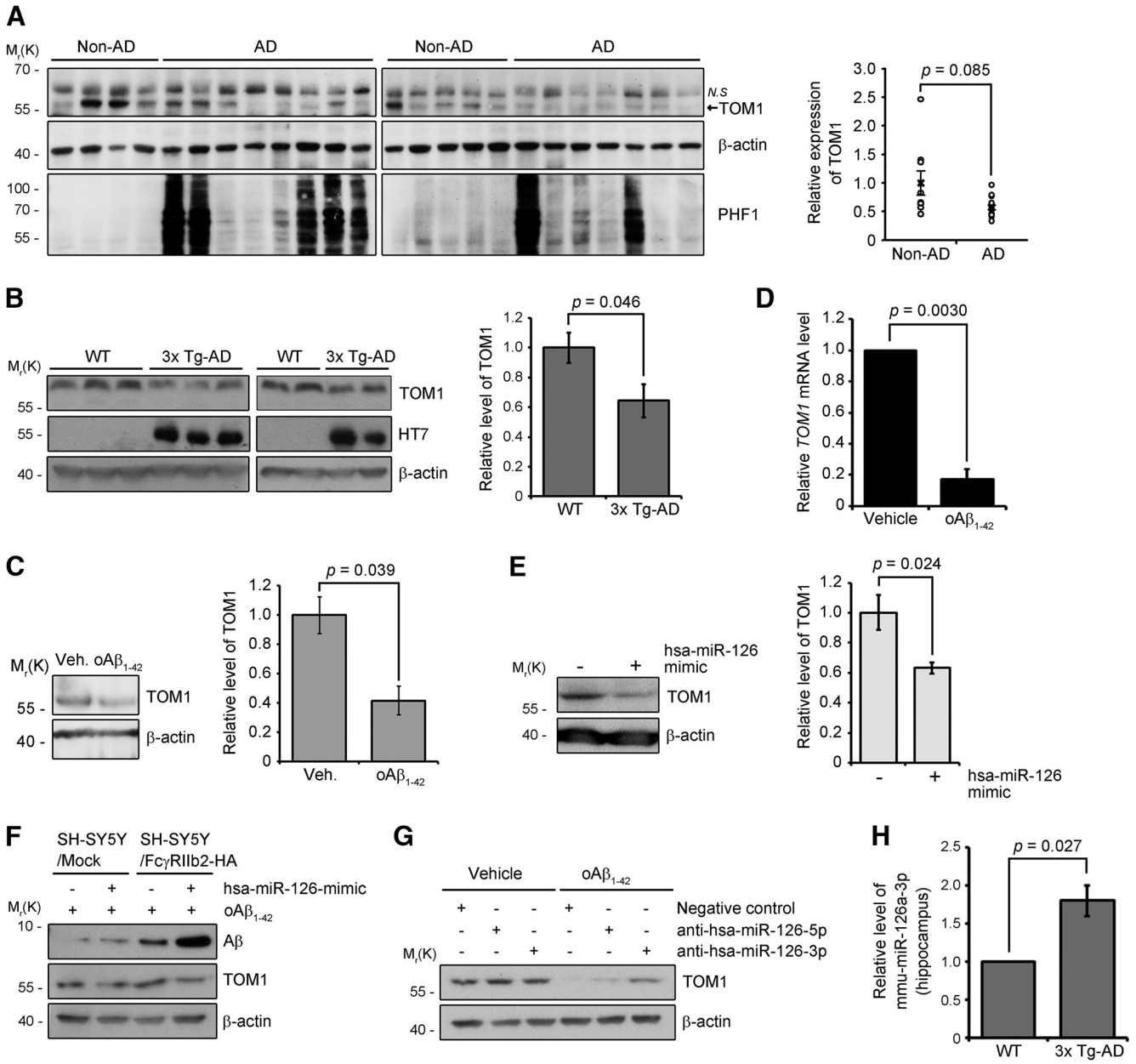

Figure 9. miR-126-3p is linked to the decline of TOM1 level by oAβ_{1-42}. ***A***, Decreased expression of TOM1 in the hippocampus of patients with AD. Hippocampal homogenates were analyzed by Western blotting (left) and the signals on the blots were quantified (right). Error bars depict mean ± SEM. t(8.64) = 1.95 (n = 9 for Non-AD controls and n = 15 for AD patients, two-tailed t test). ***B***, Western blotting showing TOM1 and tau (HT7) levels in the hippocampus of 6 month-old WT and 3xTg-AD mice (left). Error bars depict mean ± SEM. $t_{(8)} = 2.362$ (n = 5, two-tailed t test; right). ***C***, Decrease of TOM1 protein by oAβ_{1-42}. SH-SY5Y cells were treated with 1 μM oAβ_{1-42} for 24 h and analyzed by Western blotting (left). Error bars depict mean ± SEM. $t_{(4)} = 3.02$ (n = 3, two-tailed t test; right). ***D***, Decrease of *TOM1* mRNA by oAβ_{1-42}. SH-SY5Y cells were treated with PBS (vehicle) or 5 μM oAβ_{1-42} for 18 h. Level of TOM1 transcripts was analyzed by real-time PCR. Error bars depict mean ± SEM. t(2.00) = 18.069 (n = 3, two-tailed t test). ***E***, TOM1 expression is downregulated by hsa-miR-126. SH-SY5Y cells were transfected with 25 nM hsa-miR-mimic negative control or hsa-miR-126 mimic for 24 h and analyzed by Western blotting (left). Error bars depict mean ± SEM. $t_{(6)} = 3.015$ (n = 4, two-tailed t test; right). ***F***, oAβ_{1-42} uptake by FcγRIIb2 is promoted by hsa-miR-126. SH-SY5Y/Mock and SH-SY5Y/FcγRIIb2-HA cells were transfected with 25 nM has-miR-mimic negative control or hsa-miR-126 mimic for 24 h, incubated with 1 μM oAβ_{1-42} for 2 h, and then analyzed by Western blotting. ***G***, Expression of anti-miR126-3p rescues TOM1 in oAβ_{1-42}-treated cells. SH-SY5Y cells were transfected with 250 nM anti-miR negative control, anti-miR126-5p, or anti-miR126-3p for 6 h and then incubated with 5 μM oAβ_{1-42} for 18 h. ***H***, Levels of mmu-miR-126-3p in the hippocampus of 6 month-old WT and 3xTg-AD mice. Levels of mmu-miR-126-3p were measured and normalized by RNU6B. Error bars depict mean ± SEM. t(3.00) = −4.051 (n = 4, two-tailed t test).

ilar accumulation was also observed by the overexpressed FcγRIIb2, which caused massive internalization of oAβ_{1-42} (Fig. 11*D*). Accordingly, lysosomal accumulation of oAβ_{1-42} was reduced by *Fcgr2b* KO in primary hippocampal neurons (Fig. 11*E*,*F*). Collectively, excess uptake of Aβ exceeds the degrading capacity of lysosomes, causing degradation failure and accumulation in the lysosome.

As reported (Kandimalla et al., 2009; Friedrich et al., 2010), we also found significant amounts of Aβ in the mitochondria and cytoplasm in primary neurons (Fig. 11*G*). Interestingly, these subcellular localizations of Aβ were greatly reduced by *Fcgr2b* KO in the neurons. Quantitative analysis using ELISA revealed that Aβ level in the cytoplasmic sample was reduced to 20% by FcγRIIb deficiency, whereas it was 50% in the light membrane sam-

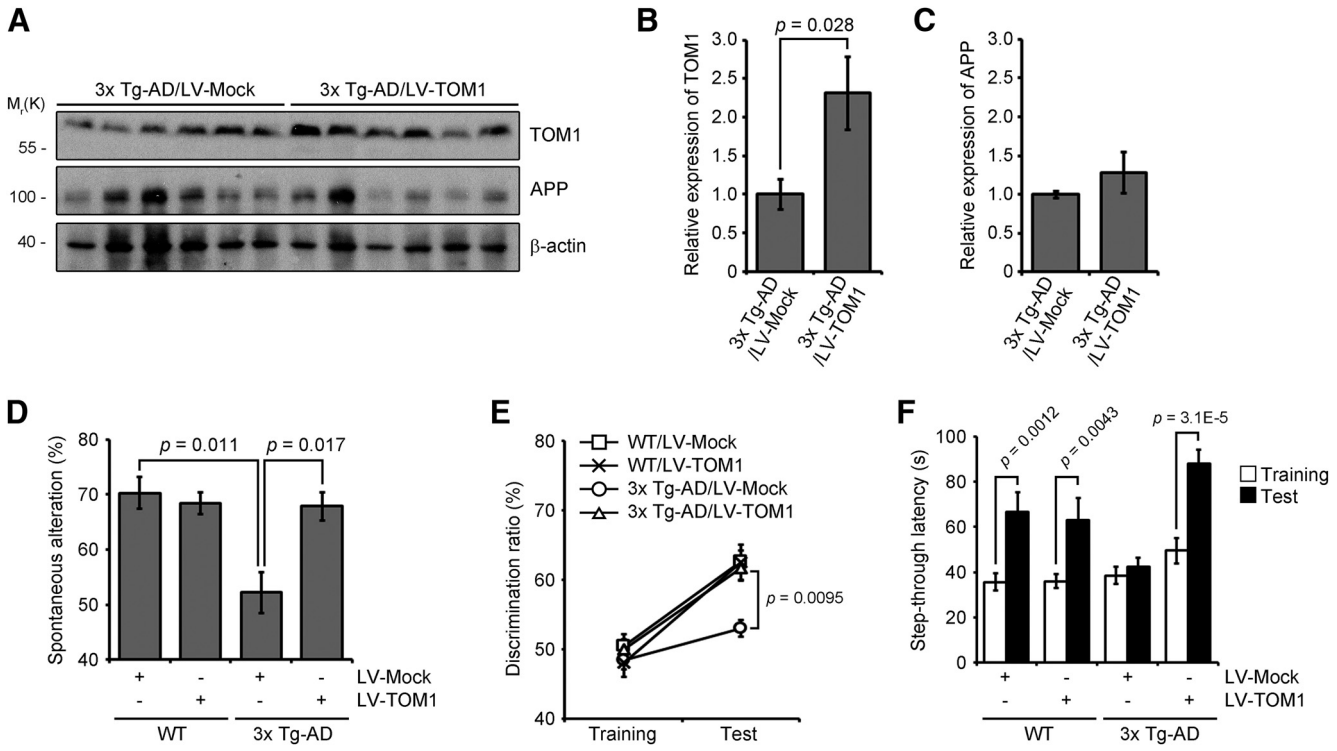

Figure 10. Amelioration of memory impairment by lentiviral transduction of TOM1 into 3xTg-AD mice. ***A–C***, Western blotting showing TOM1 and APP levels in the hippocampus of 3xTg-AD/LV-Mock and 3xTg-AD/LV-TOM1 mice (***A***). TOM1 (***B***) and APP (***C***) levels on the blots were quantified. Error bars depict mean ± SEM. $t_{(10)} = -2.566$ (***B***) and $t(5.281) = -1.034$ (***C***; $n = 6$, two-tailed *t* test). ***D–F***, Memory deficits in 3xTg-AD mice were rescued by the hippocampal expression of TOM1. Y-maze (***D***), novel object recognition (***E***), and passive avoidance (***F***) tests were performed at 1 month after injection. Error bars depict mean ± SEM. $F_{(3,26)} = 3.61$ (***D***), $F_{(7,52)} = 13.258$ (***E***), and $F_{(7,52)} = 10.032$ (***F***; $n = 7$ male WT mice for Mock virus- and TOM1 virus-injected groups, $n = 8$ male 3xTg-AD mice for Mock virus- and TOM1 virus-injected groups, one-way ANOVA with Bonferroni *post hoc* test).

ple (Fig. 11*H*,*I*). Thus, these results illustrate that FcγRIIb2 triggers the accumulation of Aβ in the mitochondria and cytoplasm as well as in the lysosome by internalizing the extracellular Aβ.

Discussion

Increasing evidence showed that Aβ is internalized into various types of cells in the brain, including neurons, astrocytes, microglia, brain microvascular endothelia, and cerebrovascular smooth muscle cells (Mohamed and Posse de Chaves, 2011; Cheung et al., 2014; Zandl-Lang et al., 2018). Nonetheless, the selectivity of Aβ species for cellular uptake into different cell types, the fate of internalized Aβ, and the pathophysiologic relevance of this process were not evaluated. The characteristics of Aβ species or strains differ from each other according to peptide length ($Aβ_{1–40}$ or $Aβ_{1–42}$), oligomeric states (monomer, low-*n* oligomer, high-*n* oligomer, or fibril), and source (synthetic Aβ, naturally secreted Aβ, or purified Aβ from pathogenic samples; Haass and Selkoe, 2007; Benilova and De Strooper, 2013). Whether internalized Aβ is subjected to either degradation or exhibits neurotoxicity is also determined by its characteristics of above and cellular capacity to defend against it. Our findings that neuron has both high capacity to internalize $oAβ_{1–42}$ and more propensity to internalize neurotoxic $oAβ_{1–42}$ than nontoxic $mAβ_{1–42}$ or $oAβ_{1–40}$ provide an intriguing model that neuron itself could be a determinant for Aβ neurotoxicity. Regarding that astrocyte prefers $mAβ_{1–42}$ to $oAβ_{1–42}$, non-neuronal cells might degrade mAβ for the clearance.

The detrimental role of intraneuronal Aβ in AD progression was previously shown in 3xTg-AD mice in which the accumulation of intraneuronal Aβ is temporally correlated with synaptic dysfunction and memory loss (Billings et al., 2005). However, there has been an issue on the pathologic role of intraneuronal Aβ in the mouse model because Aβ antibodies, such as 4G8 and 6E10, can also detect APP and its cleavage products as well as Aβ in the neurons (Lauritzen et al., 2012; Wirths et al., 2012). However, this issue does not rule out the presence of intracellular Aβ in the early age of 3xTg-AD mice. In addition, although the amount of intraneuronal Aβ is considered small, several studies suggested that the formation of amyloid seed, which leads to severe neuronal toxicity, is markedly accelerated by the locally concentrated Aβ in the acidic organelles along with endo-lysosomal track (Hu et al., 2009; Poduslo et al., 2012). Although C99 generates intraneuronal immunoreactivity in the early ages of 3xTg-AD mice (Lauritzen et al., 2012), we found no differences in the levels of APP and C99 between 3xTg-AD mice and 3xTg-AD/*Fcgr2b*-ΔCyt mice. Further, when we assessed the role of FcγRIIb2 in the toxicity triggered by C99 (Choi et al., 2007), FcγRIIb deletion was not associated with the C99-mediated neurotoxicity (data not shown). Accordingly, more evidences support the importance of intraneuronal Aβ in AD pathogenesis despite the limitation to detect intraneuronal Aβ (Iulita et al., 2014; Baker-Nigh et al., 2015).

We also found that expression of Iba1, a microglia marker, and mRNA transcripts of proinflammatory genes, such as interleukin-1 β (IL1β), inducible nitric oxide synthase, and TNFα, were more or less reduced by *Fcgr2b* KO in the cortex and hippocampus of 3xTg-AD mice (Kam et al., 2016). At this moment, we do not have any evidence showing that the non-neuronal activity of FcγRIIb is not solely responsible for the memory impairment. However, we believe that the neuroinflammation via micro-

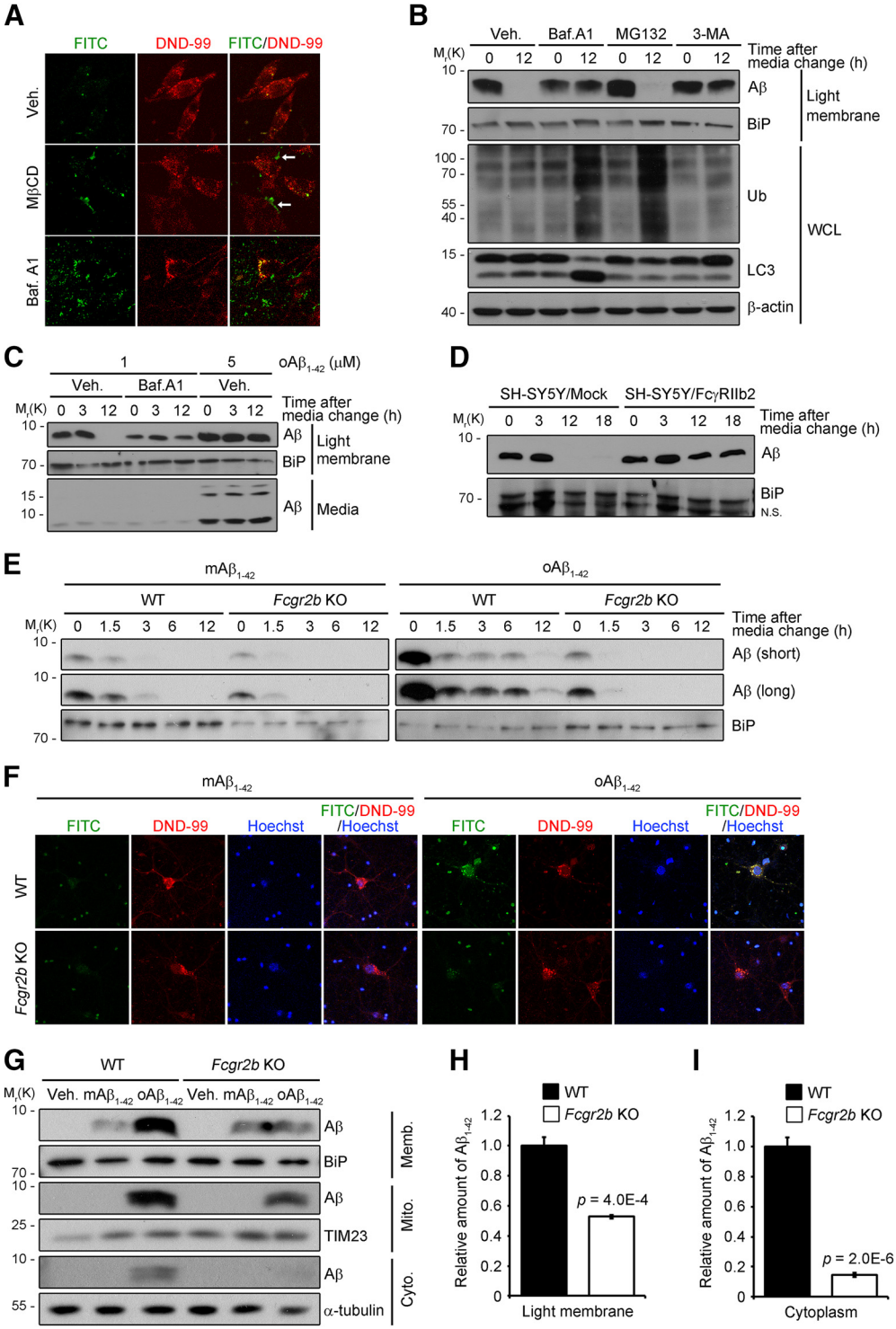

Figure 11. Promotion of oAβ_{1-42} uptake by FcγRIIb2 is linked to its cellular accumulation. ***A***, Inhibition of lysosome leads to Aβ_{1-42} accumulation in the lysosome. SH-SY5Y cells were incubated with 250 nM FITC-oAβ_{1-42} and vehicle (Veh), 0.5 mM methyl-β-cyclodextrin (MβCD), or 10 nM Baf A1 for 2 h and then treated with 50 nM Lysotracker Red (DND-99) for 1 h. Arrows indicate stacked Aβ in the plasma membrane by endocytosis inhibition. ***B***, Inhibition of lysosomal activity prevents degradation of the internalized Aβ. SH-SY5Y cells were treated with 1 μM oAβ_{1-42} for 12 h and further incubated with Aβ_{1-42}-free medium and vehicle (Veh), 10 nM Baf A1, 2.5 μM MG132, or 5 mM 3-MA for the indicated times. Whole-cell lysates (WCL) and the light membrane samples were analyzed by Western blotting. ***C***, Distinct accumulation patterns of intraneuronal oAβ_{1-42}. SH-SY5Y cells were treated with 1 or 5 μM oAβ_{1-42} for 12 h and then incubated with Aβ_{1-42}-free medium for the indicated times in the presence of vehicle (Veh) or 10 nM Baf A1. Aβ levels in the light membrane samples and conditioned media (Media) were determined by Western blotting. ***D***, Increase of Aβ accumulation by FcγRIIb2. SH-SY5Y/Mock and SH-SY5Y/FcγRIIb2 cells were treated with 1 μM oAβ_{1-42} for 12 h and incubated with Aβ_{1-42}-free medium. Aβ levels were determined by Western blotting. ***E***, Efficient degradation of internalized Aβ in *Fcgr2b* KO neurons. WT and *Fcgr2b* KO primary neurons were treated with 1 μM mAβ_{1-42} or oAβ_{1-42} for 12 h and incubated with Aβ_{1-42}-free media. Aβ levels were determined by Western blotting. ***F***, Internalized Aβ_{1-42} accumulates in the lysosome via FcγRIIb. WT and *Fcgr2b* KO primary hippocampal neurons at 14 DIV were incubated with 1.25 μM mAβ_{1-42} or oAβ_{1-42} for 18 h and then incubated with 100 nM Lysotracker Red (DND-99) for 1 h. ***G–I***, Reduction of Aβ in cellular compartments by FcγRIIb deficiency. FcγRIIb. WT and *Fcgr2b* KO cortical neurons were treated with 1 μM mAβ_{1-42} or oAβ_{1-42} for 18 h. Aβ levels in the light membrane (Memb), mitochondrial (Mito), and cytoplasmic (Cyto) samples were determined by Western blotting (***G***) and ELISA (***H***, ***I***). Error bars in ***H*** and ***I*** depict mean ± SD. $t_{(4)} = 10.91$ (***H***) and $t_{(4)} = 44.38$ (***I***; $n = 3$, two-tailed *t* test). ***B–I***, The amounts of BiP, TIM23, and α-tubulin were measured as the loading control.

glial FcγRIIb might also contribute to the aggravation of memory impairment in AD mice. Further, the notion that soluble $A\beta_{1-42}$, but not insoluble $A\beta_{1-42}$, was reduced in 3xTg-AD mice by *Fcgr2b* KO or *Fcgr2b*-CytΔ expression suggests that intraneuronal Aβ exists as the oligomeric state or is involved in the Aβ oligomerization, consistent with the previous reports (Oddo et al., 2006; Takahashi et al., 2013). It will be interesting to evaluate this role of FcγRIIb2 in other AD mouse models, such as APP E693Δ mice that even show extensive intraneuronal Aβ phenotype and AD-like memory defect without extracellular Aβ load (Tomiyama et al., 2010).

The important question is how the internalized $oA\beta_{1-42}$ by FcγRIIb2 exhibits neurotoxicity. The process of FcγRIIb2-mediated $oA\beta_{1-42}$ uptake overlaps with or uses the di-leucine-dependent receptor-mediated endocytosis, leading to the accumulation of excess $oA\beta_{1-42}$ mainly in the lysosome and in the other cellular compartments as well. Although lysosome is an organelle for Aβ catabolism, massive influx of Aβ exceeding its capacity to degrade Aβ exhibited neurotoxicity, as shown in our assays, and caused the deregulation of lysosomal activity, as reported previously (Ling et al., 2009; Song et al., 2011). Furthermore, impairment of lysosomal activity by other factors, such as *presenilin* mutations, which is frequently observed in patients with familial AD (Lee et al., 2010), may further lower the catabolic activity against Aβ and thus increase the lysosome-associated neurotoxicity. Although we do not know the mechanism by which the internalized Aβ deregulates lysosome activity, we believe that the Aβ-induced lysosomal rupture leads to the leakage of its contents and Aβ into multivesicular body and cytoplasm (Friedrich et al., 2010; Umeda et al., 2011). Thus, cytoplasmic Aβ found in the neurons of AD patients and model mice might reflect this distribution of Aβ. Given that AD-associated neuronal damage is also associated with autophagy flux (Pickford et al., 2008; Caccamo et al., 2017), Aβ accumulation in the lysosome by the augmented uptake through FcγRIIb may play a detrimental role in neurotoxicity via blockade of autophagy.

In conclusion, we found that the FcγRIIb2 variant is indispensable for Aβ neurotoxicity by mediating the neuronal uptake and intraneuronal accumulation of $oA\beta_{1-42}$, which affects AD neuropathology.

References

Aoki M, Shimozuru M, Kikusui T, Takeuchi Y, Mori Y (2010) Sex differences in behavioral and corticosterone responses to mild stressors in ICR mice are altered by ovariectomy in peripubertal period. Zoolog Sci 27:783–789. CrossRef Medline

Baker-Nigh A, Vahedi S, Davis EG, Weintraub S, Bigio EH, Klein WL, Geula C (2015) Neuronal amyloid-beta accumulation within cholinergic basal forebrain in ageing and Alzheimer's disease. Brain 138:1722–1737. CrossRef Medline

Benilova I, De Strooper B (2013) Promiscuous Alzheimer's amyloid: yet another partner. Science 341:1354–1355. CrossRef Medline

Bergtold A, Desai DD, Gavhane A, Clynes R (2005) Cell surface recycling of internalized antigen permits dendritic cell priming of B cells. Immunity 23:503–514. CrossRef Medline

Billings LM, Oddo S, Green KN, McGaugh JL, LaFerla FM (2005) Intraneuronal Aβ causes the onset of early Alzheimer's disease-related cognitive deficits in transgenic mice. Neuron 45:675–688. CrossRef Medline

Caccamo A, Ferreira E, Branca C, Oddo S (2017) p62 Improves AD-like pathology by increasing autophagy. Mol Psychiatry 22:865–873. CrossRef Medline

Caglayan S, Takagi-Niidome S, Liao F, Carlo AS, Schmidt V, Burgert T, Kitago Y, Füchtbauer EM, Füchtbauer A, Holtzman DM, Takagi J, Willnow TE (2014) Lysosomal sorting of amyloid-beta by the SORLA receptor is impaired by a familial Alzheimer's disease mutation. Sci Transl Med 6:223ra20. CrossRef Medline

Cai Z, Liu N, Wang C, Qin B, Zhou Y, Xiao M, Chang L, Yan LJ, Zhao B (2016) Role of RAGE in Alzheimer's disease. Cell Mol Neurobiol 36:483–495. CrossRef Medline

Castello NA, Green KN, LaFerla FM (2012) Genetic knockdown of brain-derived neurotrophic factor in 3xTg-AD mice does not alter abeta or tau pathology. PLoS One 7:e39566. CrossRef Medline

Chen CL, Hou WH, Liu IH, Hsiao G, Huang SS, Huang JS (2009) Inhibitors of clathrin-dependent endocytosis enhance TGFbeta signaling and responses. J Cell Sci 122:1863–1871. CrossRef Medline

Cheung C, Goh YT, Zhang J, Wu C, Guccione E (2014) Modeling cerebrovascular pathophysiology in amyloid-beta metabolism using neural-crest-derived smooth muscle cells. Cell reports 9:391–401. CrossRef Medline

Choi Y, Kim HS, Shin KY, Kim EM, Kim M, Kim HS, Park CH, Jeong YH, Yoo J, Lee JP, Chang KA, Kim S, Suh YH (2007) Minocycline attenuates neuronal cell death and improves cognitive impairment in Alzheimer's disease models. Neuropsychopharmacology 32:2393–2404. CrossRef Medline

Cirrito JR, Kang JE, Lee J, Stewart FR, Verges DK, Silverio LM, Bu G, Mennerick S, Holtzman DM (2008) Endocytosis is required for synaptic activity-dependent release of amyloid-beta *in vivo*. Neuron 58:42–51. CrossRef Medline

Dementhon K, El-Kirat-Chatel S, Noël T (2012) Development of an in vitro model for the multi-parametric quantification of the cellular interactions between candida yeasts and phagocytes. PLoS One 7:e32621. CrossRef Medline

Eimer WA, Vassar R (2013) Neuron loss in the 5XFAD mouse model of Alzheimer's disease correlates with intraneuronal Aβ42 accumulation and caspase-3 activation. Mol Neurodegener 8:2. CrossRef Medline

Espéli M, Smith KG, Clatworthy MR (2016) FcγRIIB and autoimmunity. Immunol Rev 269:194–211. CrossRef Medline

Friedrich RP, Tepper K, Rönicke R, Soom M, Westermann M, Reymann K, Kaether C, Fändrich M (2010) Mechanism of amyloid plaque formation suggests an intracellular basis of Aβ pathogenicity. Proc Natl Acad Sci U S A 107:1942–1947. CrossRef Medline

Haass C, Selkoe DJ (2007) Soluble protein oligomers in neurodegeneration: lessons from the Alzheimer's amyloid β-peptide. Nat Rev Mol Cell Biol 8:101–112. CrossRef Medline

Haass C, Kaether C, Thinakaran G, Sisodia S (2012) Trafficking and proteolytic processing of APP. Cold Spring Harb Perspect Med 2:a006270. CrossRef Medline

Hu X, Crick SL, Bu G, Frieden C, Pappu RV, Lee JM (2009) Amyloid seeds formed by cellular uptake, concentration, and aggregation of the amyloid-beta peptide. Proc Natl Acad Sci U S A 106:20324–20329. CrossRef Medline

Hunter S, Indik ZK, Kim MK, Cauley MD, Park JG, Schreiber AD (1998) Inhibition of Fcγ receptor-mediated phagocytosis by a nonphagocytic Fcγ receptor. Blood 91:1762–1768. Medline

Hunziker W, Fumey C (1994) A di-leucine motif mediates endocytosis and basolateral sorting of macrophage IgG fc receptors in MDCK cells. EMBO J 13:2963–2969. Medline

Iulita MF, Allard S, Richter L, Munter LM, Ducatenzeiler A, Weise C, Do Carmo S, Klein WL, Multhaup G, Cuello AC (2014) Intracellular Aβ pathology and early cognitive impairments in a transgenic rat overexpressing human amyloid precursor protein: a multidimensional study. Acta Neuropathol Communi 2:61. CrossRef Medline

Joshi T, Ganesan LP, Cao X, Tridandapani S (2006) Molecular analysis of expression and function of hFcgammaRIIbl and b2 isoforms in myeloid cells. Mol Immunol 43:839–850. CrossRef Medline

Kam TI, Song S, Gwon Y, Park H, Yan JJ, Im I, Choi JW, Choi TY, Kim J, Song DK, Takai T, Kim YC, Kim KS, Choi SY, Choi S, Klein WL, Yuan J, Jung YK (2013) FcγRIIb mediates amyloid-beta neurotoxicity and memory impairment in Alzheimer's disease. J Clin Invest 123:2791–2802. CrossRef Medline

Kam TI, Park H, Gwon Y, Song S, Kim SH, Moon SW, Jo DG, Jung YK (2016) FcγRIIb-SHIP2 axis links Aβ to tau pathology by disrupting phosphoinositide metabolism in Alzheimer's disease model. eLife 5:e18691. CrossRef Medline

Kandimalla KK, Scott OG, Fulzele S, Davidson MW, Poduslo JF (2009) Mechanism of neuronal versus endothelial cell uptake of Alzheimer's disease amyloid beta protein. PLoS One 4:e4627. CrossRef Medline

Kanekiyo T, Bu G (2014) The low-density lipoprotein receptor-related protein 1 and amyloid-beta clearance in Alzheimer's disease. Front Aging Neurosci 6:93. CrossRef Medline

Kanekiyo T, Cirrito JR, Liu CC, Shinohara M, Li J, Schuler DR, Shinohara M, Holtzman DM, Bu G (2013) Neuronal clearance of amyloid-β by endocytic receptor LRP1. J Neurosci 33:19276–19283. CrossRef Medline

Kasahara T, Kubota M, Miyauchi T, Noda Y, Mouri A, Nabeshima T, Kato T (2006) Mice with neuron-specific accumulation of mitochondrial DNA mutations show mood disorder-like phenotypes. Mol Psychiatry 11:577–593,523. CrossRef Medline

Kim JH, Choi DJ, Jeong HK, Kim J, Kim DW, Choi SY, Park SM, Suh YH, Jou I, Joe EH (2013) DJ-1 facilitates the interaction between STAT1 and its phosphatase, SHP-1, in brain microglia and astrocytes: a novel anti-inflammatory function of DJ-1. Neurobiol Dis 60:1–10. CrossRef Medline

Kim W, Lee Y, McKenna ND, Yi M, Simunovic F, Wang Y, Kong B, Rooney RJ, Seo H, Stephens RM, Sonntag KC (2014) miR-126 contributes to Parkinson's disease by dysregulating the insulin-like growth factor/phosphoinositide 3-kinase signaling. Neurobiol Aging 35:1712–1721. CrossRef Medline

Kim W, Noh H, Lee Y, Jeon J, Shanmugavadivu A, McPhie DL, Kim KS, Cohen BM, Seo H, Sonntag KC (2016) MiR-126 regulates growth factor activities and vulnerability to toxic insult in neurons. Mol Neurobiol 53:95–108. CrossRef Medline

Koss DJ, Jones G, Cranston A, Gardner H, Kanaan NM, Platt B (2016) Soluble pre-fibrillar tau and beta-amyloid species emerge in early human Alzheimer's disease and track disease progression and cognitive decline. Acta Neuropathol 132:875–895. CrossRef Medline

LaFerla FM, Green KN, Oddo S (2007) Intracellular amyloid-beta in Alzheimer's disease. Nat Rev Neurosci 8:499–509. CrossRef Medline

Lauritzen I, Pardossi-Piquard R, Bauer C, Brigham E, Abraham JD, Ranaldi S, Fraser P, St-George-Hyslop P, Le Thuc O, Espin V, Chami L, Dunys J, Checler F (2012) The β-secretase-derived C-terminal fragment of βAPP, C99, but not Aβ, is a key contributor to early intraneuronal lesions in triple-transgenic mouse hippocampus. J Neurosci 32:16243–16255. CrossRef Medline

Lee JH, Yu WH, Kumar A, Lee S, Mohan PS, Peterhoff CM, Wolfe DM, Martinez-Vicente M, Massey AC, Sovak G, Uchiyama Y, Westaway D, Cuervo AM, Nixon RA (2010) Lysosomal proteolysis and autophagy require presenilin 1 and are disrupted by Alzheimer-related PS1 mutations. Cell 141:1146–1158. CrossRef Medline

Lee W, Kim Y, Park J, Shim S, Lee J, Hong SH, Ahn HH, Lee H, Jung YK (2015) iRhom1 regulates proteasome activity via PAC1/2 under ER stress. Sci Rep 5:11559. CrossRef Medline

Ling D, Song HJ, Garza D, Neufeld TP, Salvaterra PM (2009) Aβ42-induced neurodegeneration via an age-dependent autophagic-lysosomal injury in *Drosophila*. PLoS One 4:e4201. CrossRef Medline

Marr RA, Rockenstein E, Mukherjee A, Kindy MS, Hersh LB, Gage FH, Verma IM, Masliah E (2003) Neprilysin gene transfer reduces human amyloid pathology in transgenic mice. J Neurosci 23:1992–1996. CrossRef Medline

Moghekar A, Rao S, Li M, Ruben D, Mammen A, Tang X, O'Brien RJ (2011) Large quantities of Aβ peptide are constitutively released during amyloid precursor protein metabolism *in vivo* and *in vitro*. J Biol Chem 286:15989–15997. CrossRef Medline

Mohamed A, Posse de Chaves E (2011) Aβ internalization by neurons and glia. Int J Alzheimers Dis 2011:127984. CrossRef Medline

Oddo S, Caccamo A, Shepherd JD, Murphy MP, Golde TE, Kayed R, Metherate R, Mattson MP, Akbari Y, LaFerla FM (2003) Triple-transgenic model of Alzheimer's disease with plaques and tangles: intracellular Aβ and synaptic dysfunction. Neuron 39:409–421. CrossRef Medline

Oddo S, Caccamo A, Tran L, Lambert MP, Glabe CG, Klein WL, LaFerla FM (2006) Temporal profile of amyloid-β (Aβ) oligomerization in an *in vivo* model of Alzheimer disease: a link between Aβ and tau pathology. J Biol Chem 281:1599–1604. CrossRef Medline

Oglesby IK, Bray IM, Chotirmall SH, Stallings RL, O'Neill SJ, McElvaney NG, Greene CM (2010) miR-126 is downregulated in cystic fibrosis airway epithelial cells and regulates TOM1 expression. J Immunol 184:1702–1709. CrossRef Medline

Oh Y, Jeon YJ, Hong GS, Kim I, Woo HN, Jung YK (2012) Regulation in the targeting of TRAIL receptor 1 to cell surface via GODZ for TRAIL sensitivity in tumor cells. Cell Death Differ 19:1196–1207. CrossRef Medline

Ovsepian SV, Herms J (2013) Drain of the brain: low-affinity p75 neurotrophin receptor affords a molecular sink for clearance of cortical amyloid beta by the cholinergic modulator system. Neurobiol Aging 34:2517–2524. CrossRef Medline

Pacheco-Quinto J, Eckman EA (2013) Endothelin-converting enzymes degrade intracellular β-amyloid produced within the endosomal/lysosomal pathway and autophagosomes. J Biol Chem 288:5606–5615. CrossRef Medline

Pickford F, Masliah E, Britschgi M, Lucin K, Narasimhan R, Jaeger PA, Small S, Spencer B, Rockenstein E, Levine B, Wyss-Coray T (2008) The autophagy-related protein beclin 1 shows reduced expression in early Alzheimer disease and regulates amyloid β accumulation in mice. J Clin Invest 118:2190–2199. CrossRef Medline

Poduslo JF, Howell KG, Olson NC, Ramirez-Alvarado M, Kandimalla KK (2012) Alzheimer's disease amyloid beta-protein mutations and deletions that define neuronal binding/internalization as early stage nonfibrillar/fibrillar aggregates and late stage fibrils. Biochemistry 51:3993–4003. CrossRef Medline

Querfurth HW, LaFerla FM (2010) Alzheimer's disease. N Engl J Med 362:329–344. CrossRef Medline

Shankar GM, Li S, Mehta TH, Garcia-Munoz A, Shepardson NE, Smith I, Brett FM, Farrell MA, Rowan MJ, Lemere CA, Regan CM, Walsh DM, Sabatini BL, Selkoe DJ (2008) Amyloid-β protein dimers isolated directly from Alzheimer's brains impair synaptic plasticity and memory. Nat Med 14:837–842. CrossRef Medline

Shin B, Oh H, Park SM, Han HE, Ye M, Song WK, Park WJ (2014) Intracellular cleavage of amyloid beta by a viral protease NIa prevents amyloid beta-mediated cytotoxicity. PLoS One 9:e98650. CrossRef Medline

Song MS, Baker GB, Todd KG, Kar S (2011) Inhibition of β-amyloid$_{1-42}$ internalization attenuates neuronal death by stabilizing the endosomal-lysosomal system in rat cortical cultured neurons. Neuroscience 178:181–188. CrossRef Medline

Sonntag KC, Woo TU, Krichevsky AM (2012) Converging miRNA functions in diverse brain disorders: a case for miR-124 and miR-126. Exp Neurol 235:427–435. CrossRef Medline

Sykora P, Misiak M, Wang Y, Ghosh S, Leandro GS, Liu D, Tian J, Baptiste BA, Cong WN, Brenerman BM, Fang E, Becker KG, Hamilton RJ, Chigurupati S, Zhang Y, Egan JM, Croteau DL, Wilson DM 3rd, Mattson MP, Bohr VA (2015) DNA polymerase β deficiency leads to neurodegeneration and exacerbates Alzheimer disease phenotypes. Nucleic Acids Res 43:943–959. CrossRef Medline

Takahashi RH, Capetillo-Zarate E, Lin MT, Milner TA, Gouras GK (2013) Accumulation of intraneuronal β-amyloid 42 peptides is associated with early changes in microtubule-associated protein 2 in neurites and synapses. PLoS One 8:e51965. CrossRef Medline

Takai T, Ono M, Hikida M, Ohmori H, Ravetch JV (1996) Augmented humoral and anaphylactic responses in FcγRII-deficient mice. Nature 379:346–349. CrossRef Medline

Takuma K, Fang F, Zhang W, Yan S, Fukuzaki E, Du H, Sosunov A, McKhann G, Funatsu Y, Nakamichi N, Nagai T, Mizoguchi H, Ibi D, Hori O, Ogawa S, Stern DM, Yamada K, Yan SS (2009) RAGE-mediated signaling contributes to intraneuronal transport of amyloid-beta and neuronal dysfunction. Proc Natl Acad Sci U S A 106:20021–20026. CrossRef Medline

Tampellini D, Rahman N, Gallo EF, Huang Z, Dumont M, Capetillo-Zarate E, Ma T, Zheng R, Lu B, Nanus DM, Lin MT, Gouras GK (2009) Synaptic activity reduces intraneuronal Aβ, promotes APP transport to synapses, and protects against Aβ-related synaptic alterations. J Neurosci 29:9704–9713. CrossRef Medline

Tomiyama T, Matsuyama S, Iso H, Umeda T, Takuma H, Ohnishi K, Ishibashi K, Teraoka R, Sakama N, Yamashita T, Nishitsuji K, Ito K, Shimada H, Lambert MP, Klein WL, Mori H (2010) A mouse model of amyloid β oligomers: their contribution to synaptic alteration, abnormal tau phosphorylation, glial activation, and neuronal loss *in vivo*. J Neurosci 30:4845–4856. CrossRef Medline

Umeda T, Tomiyama T, Sakama N, Tanaka S, Lambert MP, Klein WL, Mori H (2011) Intraneuronal amyloid β oligomers cause cell death via endo-

plasmic reticulum stress, endosomal/lysosomal leakage, and mitochondrial dysfunction *in vivo*. J Neurosci Res 89:1031–1042. CrossRef Medline

Vodopivec I, Galichet A, Knobloch M, Bierhaus A, Heizmann CW, Nitsch RM (2009) RAGE does not affect amyloid pathology in transgenic ArcAβ mice. Neurodegener Dis 6:270–280. CrossRef Medline

Walsh DM, Klyubin I, Fadeeva JV, Cullen WK, Anwyl R, Wolfe MS, Rowan MJ, Selkoe DJ (2002) Naturally secreted oligomers of amyloid beta protein potently inhibit hippocampal long-term potentiation *in vivo*. Nature 416:535–539. CrossRef Medline

Wirths O, Dins A, Bayer TA (2012) AbetaPP accumulation and/or intraneuronal amyloid-beta accumulation? The 3xTg-AD mouse model revisited. J Alzheimers Dis 28:897–904. CrossRef Medline

Yang WN, Ma KG, Chen XL, Shi LL, Bu G, Hu XD, Han H, Liu Y, Qian YH (2014) Mitogen-activated protein kinase signaling pathways are involved in regulating α7 nicotinic acetylcholine receptor-mediated amyloid-beta uptake in SH-SY5Y cells. Neuroscience 278:276–290. CrossRef Medline

Youmans KL, Tai LM, Kanekiyo T, Stine WB Jr, Michon SC, Nwabuisi-Heath E, Manelli AM, Fu Y, Riordan S, Eimer WA, Binder L, Bu G, Yu C, Hartley DM, LaDu MJ (2012) Intraneuronal Aβ detection in 5xFAD mice by a new Aβ-specific antibody. Mol Neurodegener 7:8. CrossRef Medline

Zandl-Lang M, Fanaee-Danesh E, Sun Y, Albrecher NM, Gali CC, Čančar I, Kober A, Tam-Amersdorfer C, Stracke A, Storck SM, Saeed A, Stefulj J, Pietrzik CU, Wilson MR, Björkhem I, Panzenboeck U (2018) Regulatory effects of simvastatin and apoJ on APP processing and amyloid-beta clearance in blood–brain barrier endothelial cells. Biochim Biophys Acta 1863:40–60. CrossRef Medline

Zhang CY, Booth JW (2011) Differences in endocytosis mediated by FcγRIIA and FcγRIIB2. Mol Immunol 49:329–337. CrossRef Medline .